Microstructure and segmental dynamics of industrially relevant polymer nanocomposites

Julian Oberdisse, Anne-Caroline Genix

Microstructure and segmental dynamics of industrially relevant polymer nanocomposites

Julian Oberdisse and Anne-Caroline Genix*

Laboratoire Charles Coulomb (L2C), Université de Montpellier, CNRS, F-34095 Montpellier, France

*anne-caroline.genix@umontpellier.fr

Abstract

Recent progress in the filler microstructure and the dynamical properties of polymer nanocomposites of industrial relevance is reviewed. We focus mainly on systems used in car tire treads made of styrene-butadiene rubber (SBR) matrices in which precipitated amorphous silica like Zeosil® with a complex multi-scale structure is dispersed – while occasionally comparing to other experimental systems, including model studies with well-defined colloidal silica nanoparticles. Electron microscopy and small-angle scattering – namely SAXS and SANS – are powerful methods of structural analysis, and some recent developments including the correlation hole analysis giving access to local aggregate properties, or reverse Monte Carlo approaches providing aggregate distribution functions, are discussed. The dynamical response of such complex systems is then studied by broadband dielectric spectroscopy (BDS), starting from the individual components. Maxwell-Wagner-Sillars interfacial polarization processes including charge and water migration are shown to be able to probe large-scale microstructure, evidencing filler percolation effects as observed in rheology. Then, BDS is shown to be highly suitable for studies of the evolution of the segmental dynamics of rubber, giving insight into vulcanization mechanisms under the effect of industrial additives, as well as in transitions from heterogeneous to homogeneous dynamics of polymer blends. Finally, the difficulties of investigating segmental dynamics in industrially-relevant filled systems by BDS are critically discussed, and some recent neutron spin-echo results are reported evidencing only a small impact of filler surfaces on segmental dynamics in weakly interacting SBR-silica systems.

Keywords: Small-angle scattering, reverse monte carlo, filler structure, percolation, segmental dynamics, interfacial polarization, rubber additives.

Abbreviations:

PNC: polymer nanocomposite

NP: nanoparticle

SAXS: Small-angle X-ray scattering

SANS: Small-angle neutron scattering

RMC: Reverse monte carlo

BDS: broadband dielectric spectroscopy

MWS process: Maxwell-Wagner-Sillars process

ILM: interfacial layer model

QENS: quasi-elastic neutron scattering

NSE: Neutron spin echo

Contents

1. Introduction

2. Nanocomposite formulation

3. Overview over filler structure in industrially relevant nanocomposites

3.1 Correlation hole analysis of local NP density in model nanocomposites

3.2 Application of correlation hole analysis to simplified industrial PNCs

3.3 Impact of small molecules on nanocomposite microstructure

3.4 Complete RMC study of model system

4. Dynamical signature in industrially relevant nanocomposites probed by BDS

4.1 Dielectric response of individual components

4.2 Structure-dependent charge migration in PNCs

4.2.1 Influence of water

4.2.2 Evidence of filler percolation

4.2.3 Impact of grafting density

4.3 Segmental dynamics of rubber compounds

4.3.1 Unfilled rubbers: vulcanization and miscible rubber blends studied by BDS

4.3.1.a Following vulcanization mechanisms by dielectric spectroscopy

4.3.1.b Studying miscible rubber blends by dielectric spectroscopy

4.3.2 The complex analysis of the dynamics of filled rubber: dielectric *vs.* neutron spectroscopy

4.3.2.a Dielectric and neutron spin-echo spectroscopy applied to simplified industrial systems

4.3.2.b Studying in-situ adsorption of small molecules onto filler particles by dielectric spectroscopy

5. Conclusion

1. Introduction

Polymer nanocomposites (PNCs) are fascinating materials which display unique macroscopic and microscopic dynamical properties the secret of which lies in the details of their organization on the nanoscale. They are usually made of nanoparticles (NPs) dispersed in a polymer matrix. Most common filler particles are carbon black and silica, while industrially-relevant polymers are usually rubbery, i.e. with a T_g below room temperature. In general, the matrix is crosslinked in order to limit flow of the material, but in some fundamental studies including ours, crosslinking is avoided. In industrial applications like tire treads, original material was natural rubber (NR) made of Hevea Brasiliensis latex, but geopolitical evolutions during the 20^{th} century made industry turn to synthetic polymers, in particular petrol-based polyisoprene and styrene-butadiene rubber (SBR), before becoming now again interested in NR under the pressure of environmental issues.

The dynamical properties of PNCs extend over many orders of magnitude in the frequency domain, covering the entire field from rheology related to chain reptation and flow, to mechanical behavior controlled by rubber elasticity and segmental dynamics. Obviously, the relevant frequencies for industrial applications like car tires are related to the rotational speed of the tire used in the rubbery regime. Unwanted viscous losses on this scale transform the kinetic energy of the car into heat, and thus cause the rolling resistance, which ultimately increases fuel consumption and CO_2 production. At higher frequency related to fast material deformations on the rugosity of the road, the tire needs to be dissipative, as only this property makes it stick to the road. Such wet skid properties enable the driver to break and steer under unfavorable meteorological conditions, which are after all desired capabilities that we are willing to pay for in terms of higher fuel consumption. To see this, just imagine a tire entirely made of steel – its dissipation would be zero, and the driver would be happy as long as he does not have to turn… As a result of such considerations, the fundamental dynamical properties of rubber materials on the nano- and microscale need to be understood, and tuned, in order to optimize macroscopic rheological properties. As the pure polymer matrix would be not stiff enough for applications, it is blended with hard nanoparticle fillers – taking advantage of the so-called reinforcement effect [1, 2]. The magnitude of the latter depends on many parameters, the most important one being the amount of hard material, followed by its spatial organization, and connection to the matrix polymer. The choice of the filler material has been restricted for a century to different grades of the same substance, carbon black. The latter is hydrophobic and it has strong attractive interactions with most polymer molecules, and is thus easily miscible with matrices. A lower rolling resistance of tire treads formulated with blends of SBR and BR (butadiene rubber) is however achieved using chemically coupled hydrophilic silica as reinforcing filler instead of the traditional physically coupled carbon black. This change in formulation has found its way into the commercial application through the “Michelin green tire” some thirty years ago. Nanoscale dynamics depends thus on various parameters linked to the filler structure and chemistry, and of course also to the details of

the polymer matrix itself: its chemistry, possibly blending, crosslinking, plasticization, and the impact of any additive. Moreover, the mechanical response of the material depends also in a non-linear manner on the imposed strain. These effects, in particular strain softening called the Payne effect [3, 4], are thought to be due to the filler reorganization undergone by the material under deformation. Although they are not the heart of our review, we will point out some of these aspects when appropriate for the present chapter.

Before doing so, a few definitions will be necessary. First of all, while we will focus on systems of industrial relevance, the comparison to model systems will come in handy. The idea is that real industrial systems are highly complicated, which makes physical understanding hard to achieve [5]. We therefore concentrate either on simplified-industrial systems with reduced numbers of components, but employing industrial silica filler of complex multi-scale structure, or on model systems based on colloidal silica NPs of well-defined spherical shape and size. Due to their origin, industrial filler is usually a powder which is dispersed in the polymer in an internal mixer, a process termed solid-state mixing. On the other hand, the colloidal particles are suspended in a solvent, and samples are made by solvent casting. In all cases of our studies reported here, the polymer is a well-defined, low-polydispersity styrene-butadiene, so the system remains "model" in all cases in this respect. The interaction between the polymer and the particles may be tuned, e.g. by covalent grafting of SBR, or by the amount of coating agent. In addition to this, changing the chemistry of the polymer molecules allows modifying the interactions from basically "neutral" van der Waals interactions to attractive interactions possibly based on hydrogen bonding, accompanied usually by an increased glass-transition temperature, T_g. Obviously, switching to high-T_g, glassy materials opens the road to entirely new studies, where the stronger interactions lead to well-defined interfacial regions of new physical properties. While we refer the interested reader to the chapter by A. P. Sokolov, this domain remains outside the scope of this chapter focusing on rubber systems. It is only noted that standard physico-chemical methods like the determination of bound rubber, differential scanning calorimetry (DSC), nuclear magnetic resonance (NMR) and of course broadband dielectric spectroscopy (BDS), give experimental access to such properties.

Our rationale is to develop understanding on model systems, propose innovative methodological advances, and then transpose this to the simplified-industrial system. It is thus mandatory to be able to design samples in a highly controlled manner, and then study their structure and dynamics, in order to extract correlations between parameters and properties, and ultimately gain insight in the underlying processes. Concerning the structure, our group has a strong background in scattering techniques (light, X-rays, neutrons). Scattering gives access to correlations in space and time, and depending on the design of the contrast situation, one may study NPs, or the polymer, or cross-correlations between both. In standard polymer-NP contrast, small-angle X-ray scattering (SAXS) is the method of choice.

It allows characterizing individual filler NP dispersions, the formation of aggregates, or of networks. It can be combined sometimes to transmission electron microscopy (TEM), which is sensitive to the same contrast between particles and polymer. Although it is a fascinating topic, chain structure will not be discussed in this chapter [6]. It is the realm of neutron scattering, in particular SANS, with isotopic substitution of the polymer in order to label certain polymer chains, i.e. provide contrast by chemical design. Whatever the technique, the resulting intensity functions in reciprocal space are not straightforward to interpret. In the past, our group has proposed a variety of approaches giving quantitative access to NP structure in PNCs, and some of them are briefly outlined in this chapter.

Knowing the statistical properties of the NP dispersion allows one to imagine on which spatial scale dynamical processes take place. Different methods of characterization of dynamics have been used in the literature, and here we focus mainly on BDS, with some excursions into NMR, neutron spin-echo (NSE) and rheology. These techniques give access to various processes, like segmental motion of molecules or migration of charges. Our proposition is to combine them with the static properties, for instance imagining surface motion of ions along silica structures spanning the sample by analysis of the interfacial polarization.

The organization of this chapter serves the following scope: by putting together in a step-by-step approach structural and dynamical information available on all compounds and their blends, we wish to reach the difficult discussion of segmental dynamics in rubber nanocomposites. We therefore start with section 2 which is devoted to the formulation of industrially-relevant PNCs. In section 3, we introduce our own recent contributions on filler structure in both model and industrial nanocomposites. Filler dispersion as characterized by scattering techniques like SAXS sets the landscape in which dynamical processes can take place. It is emphasized that the difficulty here does not lie in performing the experiments themselves, but in the developments of new quantitative data analyses, namely the so-call correlation-hole approach giving access to internal densities and filler aggregate masses, and thus space-filling properties up to percolation. In section 4, the dynamical features of industrially relevant PNCs are discussed, first in terms of their individual components – filler and polymer –, followed by an analysis of interfacial polarization of embedded filler described by Maxwell-Wagner-Sillars (MWS) processes. The latter include large-scale charge migration along the filler surfaces, and can thus be used as a probe of filler structure in the matrix, which evolves as a function of, e.g., filler content, or grafting. In the last part of section 4, segmental dynamics of the polymer matrix are reviewed. Its sensitivity to additives allows fine-tuning vulcanization and the glass transition, and thus macroscopic rheological properties relevant for applications. Moreover, blending of different polymer molecules with their individual relaxation processes may or may not result in blending at the molecular level leading to a single relaxation. One of the key questions of the community refers to the influence of the filler surfaces on the polymer dynamics [7, 8], and some recent progress – including quasi-elastic neutron scattering (QENS) measurements – will be discussed. Different applications of

dielectric spectroscopy, like nanoscale resolution, and a surprising measurement of the adsorption isotherm of coating agents onto silica buried in the polymer matrix will also be mentioned.

2. Nanocomposite formulation

Samples related to industrial applications are usually designed in a way to resemble as much as possible the material finally used. Experimental studies of the structure and dynamics of such samples start by carefully formulating samples of complex composition, with many ingredients [9]. Among them, the foremost ones are obviously the rubber and the filler. Rubbers refer to a class of polymers with specific elastic properties that are entropic in nature, and the ability to sustain reversibly large deformations. They are made of long and flexible chains without bulky side groups, which is the reason why their T_g is significantly below room temperature. The vast majority of rubbers is formed by addition of conjugated dienes as it is the case for natural rubber or its synthetic counterpart polyisoprene, and butadiene rubber, or by statistical copolymerization of diene and non-diene monomers as for SBR. In this chapter, our main focus lies on SBR-based PNC but some examples based on NR or BR will be discussed. Regarding the industrial filler, we restrict ourselves to precipitated amorphous silica forming breakable agglomerates of ca. 100 µm size in a dried powder. Typical radius of the elementary silica NPs is in the 10 – 20 nm range. The polymer-filler interaction is an important parameter in system design as it has direct consequence on both structural and dynamical properties. It can be tuned with coating or coupling agents. Functionalized polymer chains that are able to graft onto the silica surface during the hot mixing process are also commonly used. In the following, the label F- is added to the polymer acronym to highlight the presence of such chains in PNC (e.g., F-SBR). Interaction between polymer chains and silica surface-silanols is thus either covalent grafting via the functionalized chain-ends or a coupling agent, or weak non-specific van der Waals interactions favouring aggregation of bare silica NPs [10]. Surface modification using a coating agent is an intermediate situation allowing to reduce the filler-filler interaction, without chemical linkage with the polymer.

Rubber PNCs are prepared by solid-phase mixing using an internal mixer and/or an open two-roll mill. The different ingredients including liquid additives are introduced in subsequent steps. To improve rubber properties, the polymer chains are vulcanized, i.e., crosslinked with permanent covalent bonds using sulfur. However, this chemical process is slow and several additives termed accelerators and activators have to be included during mixing to reduce cure time and increase the reaction efficiency. The most common activators are metal oxides and fatty acids, whereas thiazoles and sulfonamides are often used as accelerators in combination with a basic molecule like diphenyl guanidine (DPG) acting as secondary accelerator. In Table 1, most common additives to SBR-silica PNCs as used in the literature are summarized.

Table 1. List of typical tire tread additives that are important for rubber processing, their abbreviation, name, and function. In the last column, their presence in industrial-simplified systems is indicated.

Additive	Full name	Function	Simplified system
IPPD	N-isopropyl-N'-phenyl-para-phenylenediamine	Antioxidant	
6PPD	N-(1,3-dimethylbutyl)-N'-phenyl-para-phenylenediamine	Antioxidant	X
AO2246	2,2'-methylenebis-(4-methyl-6-tertiary-butylphenol)	Antioxidant	X
TDAE	Treated distillates aromatic extract	Extender oil	
Si69	Bis (3-triethoxysilylpropyl) tetrasulfide	Coupling agent	
Si363	3-mercaptopropyltriethoxysilane reacted with ethoxylated C_{13}-alcohol	Coupling agent	
Octeo	Octyl-triethoxysilane	Coating agent	X
S	Sulphur	Cross-linking agent	
ZnO	Zinc oxide particles	Cure activator	
SA	Stearic acids	Cure activator	
MBTS	Bis(2-benzothiazole) disulfide	Cure accelerator	
TBBS	N-butyl-2-benzothiazole sulfonamide	Cure accelerator	
CBS	N-cyclohexyl-2-benzothiazole sulfonamide	Cure accelerator	
DPG	Diphenyl guanidine	Secondary cure accelerator	X

Nowadays, it is worth noting that the usefulness of most additives is well-motivated as their role (e.g., curative or antioxydant) has been widely studied in the literature. However, the combination of certain molecules incorporated jointly may provoke additional effects which have not been studied specifically as demonstrated in the next section for a coating agent with DPG. The association of these two chemicals commonly used in industrial formulations impacts the filler structure, which has been specifically studied by us using a new structural model discussed below [11].

In our recent studies, we have taken the approach opposite to the idea of making our systems resemble the complex real samples: nanocomposites are chosen to be as simple as possible, hence called simplified-industrial PNCs [12, 13]. In particular, care was taken not to introduce any trace of carbon black, ZnO nanoparticles, or crosslinking agents, which may render the interpretation of X-ray scattering experiments very difficult – just think of the strong scattering contribution of ZnO. Our samples are made of linear styrene-butadiene chains (SB, or SBR, if one wishes to emphasize absence or presence of crosslinking), of well-defined masses (typically between 100 and 200 kg/mol, PI below 1.1), possibly end-functionalized, in which silica NPs are dispersed. The fraction of functionalized chains among all chains is termed the F/NF fraction, or called %D3 in some of our articles. Concerning the silica, we used Zeosil 1165 MP from Solvay (of specific surface 160 m^2/g) [14], which is dispersed by internal mixing (Haake) in the polymer. A silane coating agent termed "octeo", and DPG (see Table 1) were also added, thus approaching the formulation of industrial systems, in particular in terms of structural complexity of the filler. In the specific case of swelling studies crosslinking has been introduced [15], as well as some cross-checks of its effect in [11]. Apart from this Zeosil-based system corresponding to our "simplified-industrial" one, we have set up an equivalent "model PNC" system using the same SB polymer but with colloidal silica NPs (of radius

also ca. 10 nm). These model NPs are well-defined particles of low polydispersity, which are dispersed in the polymer by solvent casting, i.e. mixing in suspension with polymer solutions in a common solvent, and drying. The main advantage of the colloidal NPs is that their scattering contribution is well-known, and one can build on it for a more complex analysis.

3. Overview over filler structure in industrially relevant nanocomposites

The filler structure of "simplified-industrial systems" as described above with ingredients limited to a strict minimum is nonetheless quite complex, due to the multi-scale structure of the industrial silica. Two methods have been combined in a quantitative way, TEM and SAXS. While the former provides an intuitive analysis but has limited representativity of local details, the latter is highly representative but technically complicated to analyze. As often in such cases, it is good practice to observe the evolution of the signals by varying a single control parameter. We have thus progressively studied the influence of silica volume fraction [12], chain functionalization [16], and chain mass [17]. In a second set of experiments, the influence of small molecules was studied [11], before extending our studies to dynamical properties (see section 4).

In the methodological development described in the following paragraphs, different levels of spatial organization need to be analyzed: at the lowest level, the primary silica particles interact to form aggregates. The aggregate size is rather easily determined from a Kratky plot, i.e. a presentation of $q^2I(q)$ *vs*. q, giving the q-position of maximum corresponding to a break in slope in the intensity I(q) – an example is given below [12]. Aggregate polydispersity has to be assumed, and we have always taken 30% – modifying this number would slightly shift results, but not change the tendencies. The mass of the aggregates, i.e. the aggregation number, can only be extracted from an intensity argument, i.e., the height of I(q). It gives access to the internal silica volume fraction of aggregates, which we call the compacity κ, and which is a key parameter for later understanding their mechanical properties. In practice, the height of the signal is related both to the aggregate mass, and to their interactions, expressed by the inter-aggregate structure factor. The latter depends in a crucial way on the aggregate volume fraction (related to the number of aggregates per unit volume), not to be confused with their (internal) κ, and for which a quantitative analysis of many TEM-images was necessary. It gave access to the large-scale filler structure in terms of branches and sheets densely filled with aggregates. Altogether, this opens the road to what we termed a correlation hole analysis giving the volume fraction of aggregates, and thus their interactions, their mass, and finally compacity. The main ideas are outlined below, dividing the task in two parts. First the interplay between the local NP density and the resulting interaction measured in a scattering experiment and expressed by the correlation hole is conceptually introduced for model particles. In a second step, it is applied to industrially-relevant

PNCs, where the interaction takes place on two structural levels, within aggregates, and between aggregates.

3.1 Correlation hole analysis of local NP density in model nanocomposites

While the idea to take interactions into account was originally motivated by our first studies of simplified-industrial PNCs as a function of silica fraction [12], a general model approach has been proposed by us only a few years later [18]. The idea was taken up recently by Arleth and Pedersen within a generalized description of structure factors [19]. An empirical description of particle interactions within aggregates has also been included by Beaucage in his famous multi-scale fractal description of scattering of aggregates [20, 21]. In our studies, adding more filler led obviously to stronger local interactions, but they had never been described quantitatively in the literature before for complex filler NPs of industrial origin.

In order to understand the concept, one can start by looking at the hard-sphere structure factor S(q), i.e. the Fourier transform of the pair correlation function of spheres suspended in a solvent and which possess excluded volume corresponding to their size, and no other long-range interaction. Such a structure factor influences the scattering I(q) by introducing a multiplicative term to the form factor P(q), which describes the particle shape. For monodisperse particles – monodispersity is only assumed for the sake of a simplified discussion, our analysis always includes polydispersity –, the intensity reads:

$$I(q) = \Phi_{NP}\, \Delta\rho^{2}\, V\, S(q)\, P(q) \qquad (1)$$

where Φ_{NP} is the volume fraction of nanoparticles, $\Delta\rho$ their scattering contrast (in cm^{-2}), and V their volume. P(q) is normed to one at low q for convenience, while S(q) is normed to one at high q by definition [22]. If one looks at the shape of S(q) for hard spheres, it has a low-q limit which is below one, and which is the normalized isothermal compressibility of the gas of spheres. S(q) can be calculated analytically in this case, and the so-called Percus-Yevick structure factor [23, 24] has the following low-q limit:

$$S_{PY}(q \to 0) = \frac{\left(1 - \alpha\, \Phi_{NP}\right)^{4}}{\left(1 + 2\,\alpha\, \Phi_{NP}\right)^{2}} \qquad (2)$$

where α is a prefactor of the volume fraction. It depends on particle polydispersity, and for monodisperse spheres, α equals 1. The conclusion is that measuring the low-q limit of the structure factor gives access to the particle volume fraction Φ_{NP}! And conversely, any intensity measured in this range is affected by S(q), and the particle (or aggregate) volume V in Eq. (1) can only be extracted quantitatively if a trustworthy estimate of S(q) is available.

The next step is to consider aggregates as depicted in the inset of Figure 1. Note that all our calculations include particle polydispersity denoted as σ, and numerical results have been obtained by averaging over many such aggregates. The resulting average scattering function I(q) is seen to start at low-q from a high number which is related to the total aggregate mass. It then decreases following what is called a Guinier regime, proportional to a Gaussian function of parameter R_g, i.e. the radius of gyration of the aggregate. It finally meets the particle form factor P(q) in the intermediate and high q-range, where I(q) and P(q) perfectly superimpose. Using Eq. (1), one can calculate and plot the apparent structure factor S(q) of the aggregates. Its shape has three different regimes: the same Guinier regime at low-q related to the aggregate size and volume, a high-q regime where it tends to one, and a depression around q* which is the correlation hole we are interested in. This is the manifestation of Eq. (2) for a system (i.e. an aggregate) of finite size. By measuring its depth S(q*), one can extract the internal volume fraction κ of the aggregate, provided one knows α in Eq. (2) as a function of particle polydispersity.

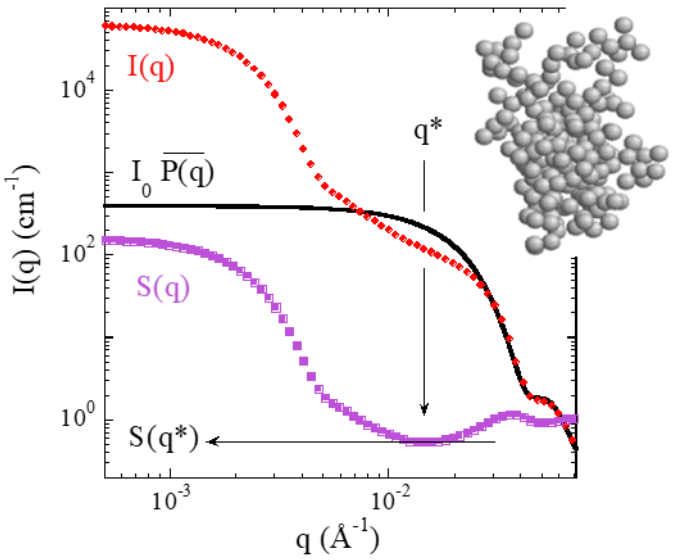

Fig. 1. Average intensity I(q) (circles), the average NP form factor P(q) (solid line), and the resulting apparent S(q) (squares) as a function of wave vector q of simulated individual aggregates containing 200 polydisperse NPs (R_0 = 10 nm, σ = 15%). Inset: example of aggregate. q* indicates the position of the correlation hole, and S(q*) its value. Adapted from [18].

The question to be answered is thus to calculate α for well-known particle densities within aggregates. We have thus generated and equilibrated very big ("infinite" on our scale) homogeneous system of repulsive spheres of average volume fraction Φ_{NP}, as shown in the cubic simulation box in the inset of Figure 2a. The compressibility is a function of this global volume fraction, and if one cuts a spherical piece out of this representing an aggregate, then the local volume fraction $\kappa = \Phi_{NP}$, the compacity, is related to the depth of the correlation hole. Due to the finite size of such aggregates, the low-q structure factor increases up to a high value related to the number of spheres in the aggregate, i.e. to

the aggregation number. Due to the aggregate of well-defined spherical shape, typical aggregate form factor oscillations are found in the intermediate q-range. The correlation hole, as shown in Figure 2a, corresponds to the minimum of the envelope of the aggregate form factor oscillations. The higher the internal aggregate concentration, the deeper the correlation hole S(q*), as shown exemplarily for two Φ_{NP}-values, 20% and 40%. In Figure 2b, S(q*) is plotted as a function of κ for different log-normal particle polydispersities. These function can be fitted using Eq. (2), and α(σ) has been reported in [18]. As a result, it is thus possible to relate the observed correlation hole to the internal density, and thus to the average aggregate mass, if the size is known from a Kratky plot. Moreover, using simulated aggregates which we could characterize extensively in real space before extracting their compacity from their (calculated) scattering, we have been able to confirm the proposed "correlation hole" approach [18].

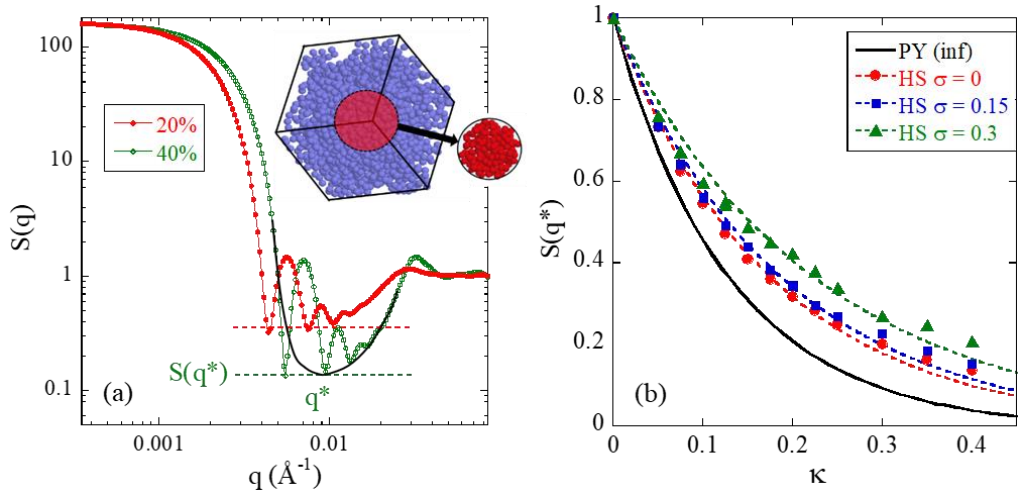

Fig. 2. a Structure factor S(q) of finite spherical systems made of hard spheres, for two local volume fractions, κ = 20 and 40% (polydispersity σ = 15%) generated by setting κ = Φ_{NP}. q* represents the position of the correlation hole, the continuous black line illustrates its average shape. Inset: "Infinite" simulation box with equilibrated hard spheres, and illustration of cutting out a finite spherical aggregate in the box center. **b** Low-q structure factor S(q*) of finite spherical systems as a function of κ based on simulations of hard spheres (σ = 0, 15, 30%). Dotted lines are fits using Eq. (2) with α = 0.73, 0.69, and 0.57, for σ = 0, 15, and 30%, respectively. The solid line is the (infinite) Percus-Yevick prediction. Adapted from [18].

As a last point on this conceptual approach, the reader might wonder why the mass and density information is not extracted from the low-q Guinier scattering, where the aggregate radius of gyration and mass are measured. The reason is that in real systems, there is more than one aggregate, and the more interesting a system is, the more aggregates there are, in close vicinity, and thus interacting. This higher level of interaction modifies the low-q scattering such that the Guinier regime is eventually masked.

3.2 Application of correlation hole analysis to simplified industrial PNCs

In industrially relevant nanocomposites, a first level of interaction corresponds to the formation of aggregates by nanoparticles. It results in a correlation hole as described above. However, this is superimposed by a higher level of organization caused by the repulsive interaction of aggregates within dense branches or sheets. This second level of correlation hole analysis needs additional information on the presence of voids in the sample, or inversely, the volume of the branches and sheets, which are visible in TEM and have been quantified by image analysis and averages over many images. Aggregates are thus themselves concentrated in large-scale fractal branches or sheets of lateral thickness of ca. 150 nm, extending over microns. This is illustrated in Figure 3a.

The multi-scale filler structure of the Zeosil 1165 MP has been modelled starting with the primary silica beads as basic building units. Their scattering analysis reveals a lognormal filler size distribution (R_0 = 8.55 nm, σ = 27%, giving an average radius $<R_{NP}>$ of 8.9 nm and an average bead volume of V_{NP} = 3.6 10^3 nm^3), in agreement with TEM studies. V_{NP} allows estimating aggregation numbers of silica NPs within aggregates. The typical radius of these aggregates found from Kratky plots ($q^2I(q)$ vs q) is in the 40 nm range. These sizes are found in the scattered intensity in Figure 3b, where the breaks in slope corresponding to the nanoparticles, the aggregates, and the branches are identified by arrows. Aggregates repel each other, thus introducing a correlation hole effect as introduced in section 3.1, which is illustrated by the arrow with increasing Φ_{NP} in Figure 3b. In this normalized representation of $I(q)/\Phi_{NP}$, the increase of silica concentration leads to a decrease of the signal in the intermediate q-range, reinforcing the correlation hole. As shown above, its depth is directly related to the concentration of aggregates after subtracting a low-q power law associated with the surface scattering of branches. The aggregate content is higher than the nominal silica volume fraction due to the confinement within the fractal sheets, the remaining space being occupied by the polymer. Applying Eq. (2) with parameters given in [12] provides the aggregate volume fraction in the sheets/branches, and thus together with the conservation law of silica the aggregate mass and internal compacity κ. Resulting values are in the 30% to 40% range, depending on the formulation, which corresponds to aggregation numbers of some 50 NPs. The latter does not depend strongly on the silica content, which was a surprising result given the highly different system viscosities during mixing. Such a result was not recognized before, probably because the decrease in the low-q intensity was attributed to a decrease in aggregate mass upon mixing at higher viscosity, neglecting the correlation hole effect due to S(q) in Eq. (1). It is also noteworthy that mechanical measurements could be described using the average aggregate compacity reported here [12].

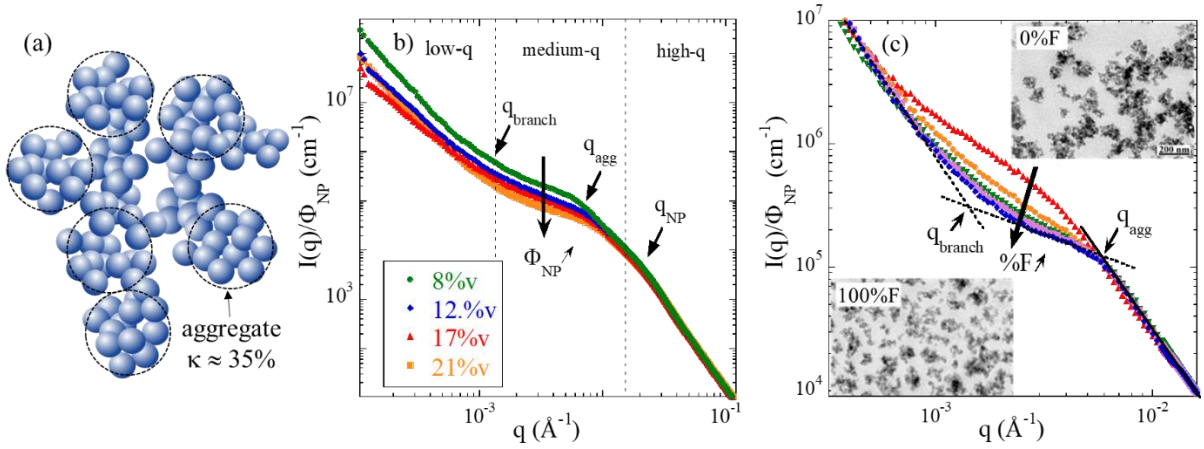

Fig. 3. a Schematic representation of the multi-scale filler structure in industrially relevant PNCs. Local aggregates are highlighted with their local density κ. **b** Silica structure via the reduced SAXS intensity, $I(q)/\Phi_{NP}$, of 50%F-PNCs (140 kg.mol^{-1}) for different silica contents Φ_{NP}, with indications of the different structural contributions. **c** Silica structure of 8.5%v-PNCs (140 kg.mol^{-1}) with different matrix compositions from 0 to 100%F. In the inset, two TEM pictures are shown, for 0% and 100%F, at $\Phi_{NP} \approx 8.5\%$v. Adapted from [12, 16].

In Figure 3c, the influence of another important control parameter on the silica structure is shown. By varying the fraction of end-functionalized chains from 0% to 100%, the inserted TEM pictures show a strong reorganization. Unfunctionalized chains induce more irregular structures, while the opposite is true for functionalized ones. In the reduced units of the X-ray scattering, the signal at intermediate q is depressed. If one takes into account the approximately constant correlation hole – these experiments are performed at fixed silica volume fraction –, the aggregate mass is found to decrease with the functionalization. The latter is thus a convenient control parameter of filler structure in complex polymer nanocomposites. It also paved the road to a more global approach, based on the grafting density of the chains on the silica [25]. Indeed, it was found that the latter determined the silica structure in a unique way (within a restricted range). Originally, this finding was triggered by the observation of very similar TEM pictures for different compositions, and gave the name to the corresponding article on "twins".

The analysis of the importance of grafting on final structure gave rise to a speculative sequence of processes during mixing – we are still hoping to study this in-situ one day. Depending on the sample viscosity defined by mainly chain mass and silica content – high viscosity favoring fragmentation –, the silica pellets are broken up finely in the internal mixer. The aggregate size thus decreases in a first moment, before a reagglomeration process sets in. The latter is driven by the attractive interactions between bare silica particles, and is impeded if chain grafting takes place. The higher the chain grafting, the lower the final aggregate masses, as described above. This mechanism is schematically shown in Figure 4.

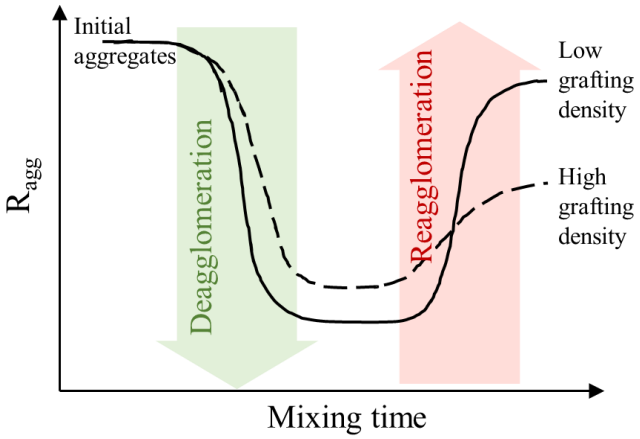

Fig. 4. Evolution of the aggregate size during the solid-state mixing process compatible with the result observed after mixing. Aggregates are thought to deagglomerate more or less depending on the viscosity of the polymer-particle blend, but reassemble in the "hot phase", in a way which is controlled by the grafting density. Adapted from [17].

For the sake of completeness, it is also mentioned that the structural studies based on the correlation-hole idea have been applied to industrial PNCs formulated with natural rubber and silica [26]. Quite some research is currently devoted to systems obtained by rapid coagulation [27], which seems to be an industrially promising way to return from synthetic to natural, bio-based, and thus sustainable materials. In the work by Boonsomwong et al. [26], the structure of such systems has been measured by SAXS, with specific attention paid to mechanical rejuvenation of the samples. The remarkable result concerning structure is that the scattered intensity I(q) overlaps over a large q-range, including the correlation hole and the high-q scattering, both for all PNCs and the primary silica powder. Without being quantitative, this is a strong indication that the local correlations between the silica NPs are not affected by any mechanical work, in particular milling. On the other hand, the low-q structure evolves with concentration and milling, showing the break-up of large-scale NP assemblies, while the Payne effect weakens simultaneously.

3.3 Impact of small molecules on nanocomposite microstructure

The effect of so-called small molecules has been studied in a second time, on virtually identical simplified-industrial PNC samples [11]. One of the most important molecules is a silane coating agent, commonly called "octeo" (see Table 1, and section 2). In Figure 5a, the reduced scattered intensity $I(q)/\Phi_{NP}$ is plotted for different amounts of octeo, the nominal value being 8% in mass with respect to the silica filler, all other parameters remaining fixed.

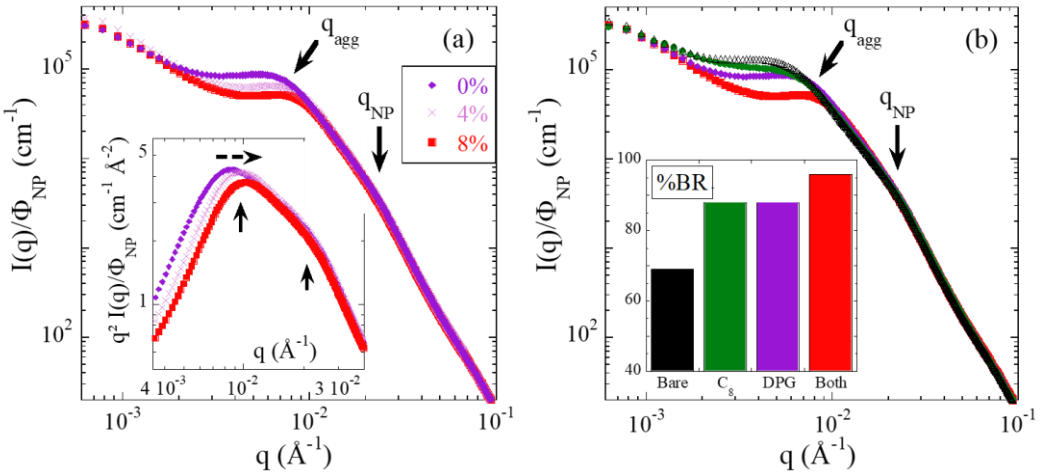

Fig. 5. Reduced SAXS intensities $I(q)/\Phi_{NP}$ allowing the structural comparison between F-SB PNCs with ca. 18%v of silica and different compositions in octeo and DPG. Arrows indicate the q-ranges of particle- and aggregate-scattering. **a** PNCs made with DPG and different amounts of octeo: 0 (diamonds), 4 (crosses), and 8%wt (squares). The inset shows the corresponding Kratky plot $q^2I(q)$ *vs.* q highlighting the structural evolution (dashed arrow). **b** PNCs made without small molecules (bare, triangles), with DPG only (diamonds), with octeo only (circles), and with both octeo and DPG (squares). The fraction of octeo (when present) is 8%wt. The inset shows the bound rubber of the same PNCs. Adapted from [11].

The scattering in Figure 5a is typical for our simplified industrial PNCs as discussed in Figure 3. The coating agent has a strong effect on the aggregate structure probed at intermediate q. The intensity levels vary considerably on this logarithmic scale. In absence of octeo, the dispersion is worst, with the highest intensity in Figure 5a, and it improves with increasing octeo content as shown by the arrow. A quantitative analysis of these data shows a decrease in aggregation number N_{agg} from some 50 to 30, accompanied by a decrease in aggregate size R_{agg} from 34 to 30 nm as one can see from the Kratky plot shown as inset. The decrease in N_{agg} indicates a higher compatibility of the filler with the matrix, as there is more polymer in contact with silica surfaces for smaller aggregates. Incidentally, this induces a higher amount of bound rubber (not shown here, [11]).

We have also studied the simultaneous effect of both the coating agent octeo, and DPG, as shown in Figure 5b. A synergetic effect is found, in the sense that none or only one of the two molecules leads to rather high scattering in the intermediate q-range, corresponding to a high aggregation number if one follows again the quantitative analysis based on the correlation hole outlined above. Only the simultaneous presence of both induces a low aggregation number and size ($N_{agg} \approx 30$, $R_{agg} = 30$ nm), and correspondingly a higher bound rubber value as shown in the inset of Figure 5b.

3.4 Complete RMC study of model system

In the preceding paragraphs, we have described how one can extract quantitative information even in complex multi-scale filler systems, in particular on aggregate sizes and their internal densities, from

small-angle scattering, with the help of large-scale image analyses based on TEM. This analysis is based on the implicit assumption that both primary particles and aggregates possess spherical symmetry, and polydispersity affects only the radii, not the shape. There is, however, no visual proof, say by imaging techniques, that this is indeed true, although such a simplified description is probably not too far from reality – after all, primary particles look somewhat "potatoe-like". If one wishes to go one step further in the calculations, one needs to step back (hopefully only momentarily) to the more ideal systems of colloidal nanoparticles. As their shape is essentially spherical and well-described by some average radius and polydispersity, such a model system is better suited for more involved calculations of scattering patterns. The reason behind this is again that Eq. (1) is strictly valid only for (monodisperse) objects of spherical symmetry. A more elaborate version of Eq. (1) for polydisperse spheres can be derived in a straightforward manner, as used by us in [12], but non spherical shapes would include computationally intractable orientational dependencies of the form and structure factors.

We have designed model PNCs based on the same SB polymer, but introducing colloidal particles of radius 12.5 nm and log-normal polydispersity 0.12. Using a reverse Monte Carlo approach [28, 29] which we have applied for the first time to individual PNC aggregates [30] and recently large-scale PNC systems [31], it is possible to explore particle configurations in space which have a scattering signal compatible with the experimentally observed intensity. Many details would need to be discussed here, but for lack of space (and adequacy of the topic) the interested reader is referred to the abovementioned literature. The most important point is that there is no unique solution to this ill-posed problem, but all solutions define a family which can be investigated statistically. For illustration, a comparison of TEM pictures with (arbitrary) slices of the simulation box containing possible configurations is shown in Figure 6a-d, for different silica fractions of the model system [31]. The "model" nature is immediately recognized in the TEM pictures, as beads are visible individually. The computer slices of same thickness as the experimental ones (70 nm) show strict polydispersity due to the plotting program. In reality, particles do have polydispersity.

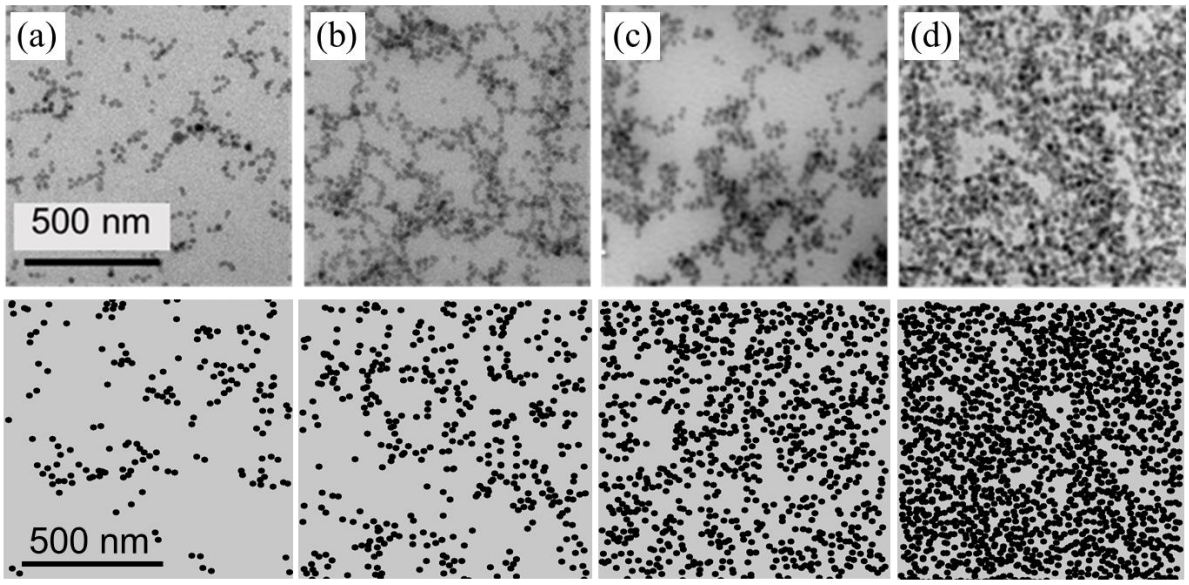

Fig. 6. Series of TEM pictures of silica-SB nanocomposites with increasing particle volume fraction Φ_{NP}. **a** 2.6%v, **b** 6.0%v, **c** 10%v, and **d** 20%v. For illustration, 70 nm-thick slices of the RMC-simulation box are shown below each picture, at the same nominal concentrations. Adapted from [32].

In Figure 6a-d, the crowding of the system, with the formation of strands and irregular aggregates is nicely reproduced by the simulation. At higher concentrations, voids or pores seem to be formed, again in agreement with the experimental result.

Once one has obtained a set of particle positions which agree with the scattering – this agreement is shown in Figure 7a where the simulation lines perfectly overlap with the experimental points – one can analyze these configurations quantitatively. An example of a simulation box is shown in the inset of Figure 7a, where an aggregate (including periodic boundary conditions) is highlighted in red. It is then possible to evaluate the aggregation number, and count the number of existing aggregates having this aggregation number. The result is an aggregate mass distribution plot as shown in Figure 7b, where one can read off how many particles are single, doublets, etc. As the concentration is increased, the reduced scattering intensity at low-q decreases again under the effect of the correlation hole. Bigger and bigger aggregates are formed, until finally almost the entire box forms a giant aggregate. This can be seen in Figure 7b by the formation of aggregates with around 10’000 NPs. It is thus interesting to see how the average aggregate mass evolves with concentration. We have proposed an indicator of aggregate mass, $\langle N_{agg}^2 \rangle / \langle N_{agg} \rangle$, which is related to the low-q intensity in polydisperse systems.

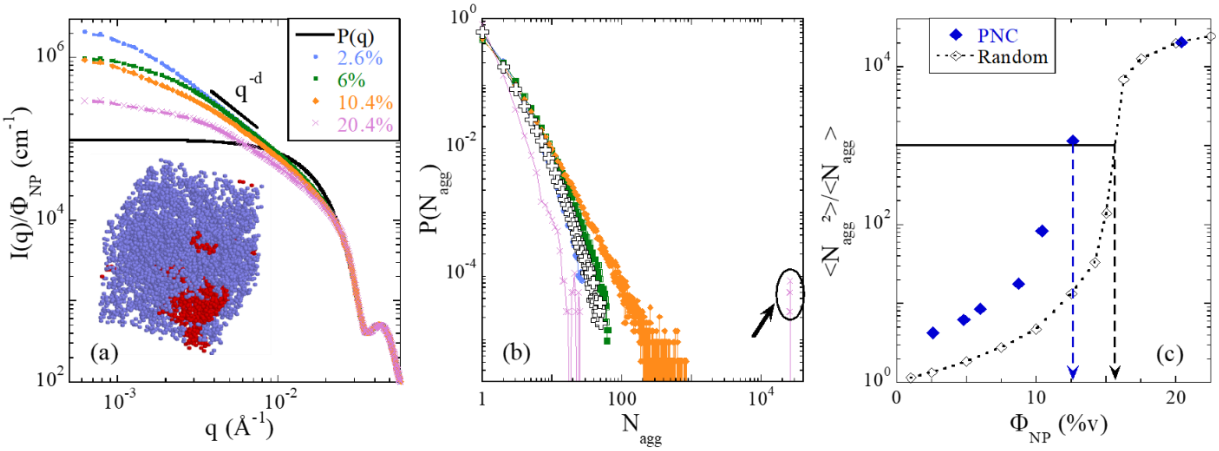

Fig. 7. a Reduced SAXS intensities $I(q)/\Phi_{NP}$ of silica-SB PNCs, for different NP volume fractions Φ_{NP}. The dotted lines superimposed to the symbols represent the result of the RMC fit. The NP form factor in polymer is represented by a black line. **b** Example of distribution functions of N_{agg} deduced from scattering normalized by the total number of aggregates in each configuration, and averaged over 100 configurations. The distribution for a random dispersion of the same NPs (Φ_{NP} = 10.4%v, δ = 0.6) is represented by black crosses. **c** Aggregation indicator $<N_{agg}^2>/<N_{agg}>$ as a function of Φ_{NP} for the silica-SB PNCs. The dotted line illustrates the aggregation of the same NPs with a random dispersion in the simulation box. The vertical arrows point toward the percolation threshold for both sets of NPs. Adapted from [32].

Plotting this indicator in Figure 7c shows the strong increase with particle volume fraction at a critical threshold, which is related to the percolation of the hard silica across the entire sample – or the simulation box on our scale. As a comparison, the indicator calculated in the same manner for a random dispersion of the same polydisperse spheres in the box is shown to have a retarded increase. This demonstrates the propensity of the NPs to aggregate, and eventually connect the entire sample, inducing mechanical percolation at lower filler content.

4. Dynamical signatures in industrially relevant nanocomposites probed by BDS

BDS is a powerful tool with a straightforward principle: a sinusoidal electric field is applied to the sample sandwiched between two flat electrodes and one measures the complex impedance leading to the dielectric permittivity as a function of temperature and frequency, possibly pressure. The main benefit of BDS applied to polymeric materials is that it allows covering a broad frequency range (10^{-2} – 10^{6} Hz in most cases). A complete dynamical process is thus captured in a single experiment, as opposed to mechanical measurements where it is generally needed to build master curves applying the time-temperature superposition principle. This is known to be problematic as soon as two processes with different T-dependence overlap. The two main polarization mechanisms responsible for the dielectric response of polymers and PNCs are the dipolar polarization due to the reorientation of permanent dipoles, and the polarization resulting from the migration of charges. Any molecular motion involving fluctuations of the dipole moments is detectable by dielectric spectroscopy as

detailed in this section. At low frequency, the motion of ionic charges (here basically residual impurities) gives rise to conductivity but also to interfacial polarization, which is predominant in composite systems and may hinder a proper characterization of the segmental relaxation. Both contributions are schematically represented in Figure 8.

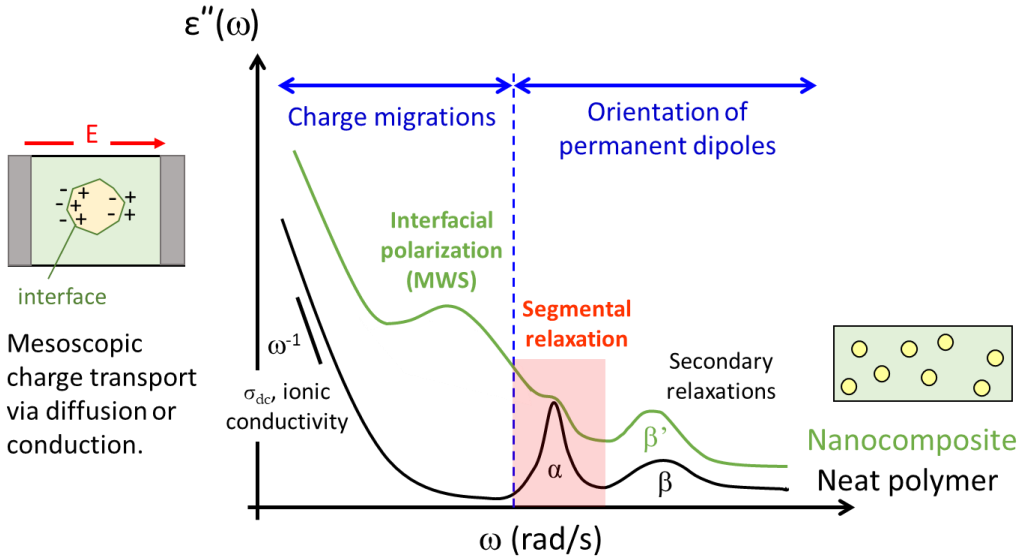

Fig. 8. Schematic overview of dynamical processes evidenced by isothermal dielectric loss spectra of polymer and polymer nanocomposites.

4.1 Dielectric response of individual components

We begin with an independent determination of the dynamics of the two main PNC components, namely the rubber matrix and the silica filler. Polymer melts display various dynamical processes depending on the probed length and time scales. Among them, the segmental dynamics (also named α-process) corresponds to the primary structural relaxation associated with the glass transition. It involves cooperative segmental motions of the polymer chain arising from conformational transitions. Figure 9 shows the typical evolution of the frequency-dependent dielectric loss for a pure styrene-butadiene random copolymer in the temperature range of the α-relaxation (typically 253 – 278 K). The position of this relaxation in the frequency window depends on the styrene content, a higher proportion of styrene units leading to higher T_g [33]. In the frequency domain, the α-relaxation is commonly described by a Havriliak-Negami (HN) function with a simultaneous fit of the imaginary and real parts of the complex permittivity

$$\varepsilon^*(\omega) = \varepsilon_\infty + \frac{\Delta\varepsilon}{[1+(i\omega\tau_{HN})^\gamma]^\delta} \quad (3)$$

where Δε is the dielectric strength, τ_{HN} the characteristic relaxation time, and γ and δ are the width and asymmetry parameters of the HN distribution, respectively. As observed for many polymers [34], the α-process of the neat SB polymer has an asymmetric shape (δ in the range 0.4 – 0.6). We found that

the shape of the distribution does not depend on functionalization of the SB chains. However, it becomes symmetric in the vulcanized system, the low-frequency side of the relaxation peak being the only part impacted by crosslinking with a slowing-down of the cooperative segmental motions [35, 36].

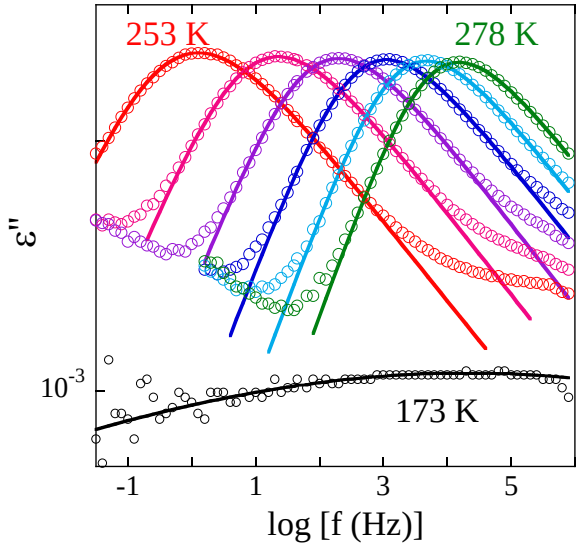

Fig. 9. Dielectric loss spectra as a function of frequency for pure F-SB between 253 K and 278 K every 5 K and at T = 173 K (black circles). Solid lines represent fits with an HN function.

On the high-frequency side of the low-temperature spectra in Figure 9, the tail of a second process is discernible. It corresponds to the secondary β-relaxation observed below T_g with a typically weak, Arrhenius T-dependence (activation energy of 32 kJ/mol). This process is perfectly observable in the frequency window at 173 K. Among the different molecular units constituting the SB chain, it has been shown that local motions of the butadiene units are responsible for the β-relaxation [33], with distinct contributions of the 1,4-*cis* and 1,2-vinyl groups on the high- and low-frequency side of the dielectric process, respectively [37].

We now turn to the precipitated silica filler. Silica NPs are hydrophilic due to the presence of a large number of silanol groups on the surface [38]. These groups promote the adsorption of water via hydrogen bonding, and humidity levels of the order of 7% have been reported for highly dispersible silica [14]. Cerveny et al. proposed a complete dielectric study of Zeosil Z1165 MP produced by Solvay, highlighting the effect of the hydration level [39]. Silanols and water molecules contribute on a similar level due to their comparable and strong dipole moment. Figure 10a shows the evolution of the dielectric loss of silica particles with different water concentrations at low temperature. Two main relaxation processes have been identified in the frequency window as illustrated in Figure 10b: a low-frequency process (called process 2 in the figure) associated with the reorientation of hydrated, vicinal and geminal, silanol groups, and a well-defined high-frequency process (termed process 1) due to the

relaxation of water molecules. The dielectric strength of the latter strongly depends on the water content with the formation of water clusters at high concentration.

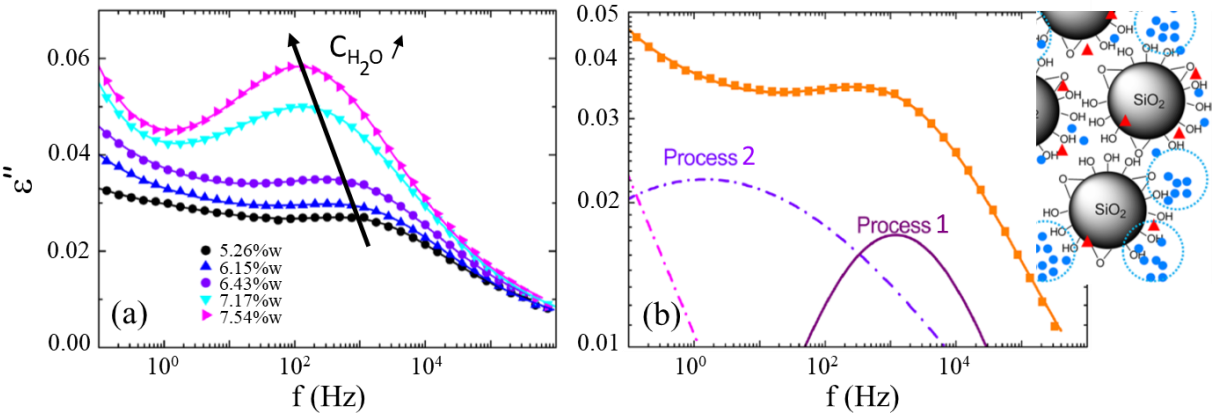

Fig. 10. Dielectric loss spectra of hydrated silica NPs at T = 146 K. The solid lines through the data points represent fits to the experimental data using the sum of two Cole-Cole functions (δ = 1 in Eq. (3)) and a conductivity term. **a** NPs at different water concentrations, **b** decomposition of the dielectric response of NPs containing 6.4%w of water. At this temperature, processes 1 (solid line, water) and 2 (dashed-dotted line, silanols) are observed. Note that they are termed processes 2 and 3, respectively, in the original publication [39]. Inset: schematic drawing of the water adsorbed at the silica surface (blue dots: hydrogen bond water, red triangles irrotational water). Water molecules are distributed homogeneously or grouped to form clusters at high concentration (dotted circles). Adapted from [39].

A similar identification of the dielectric relaxation processes of precipitated silica NPs has been made by Meier et al. in SBR nanocomposites [40] , and an overall β' process is illustrated in Figure 8 for the silica contribution. The authors studied the impact of surface modification, showing that grafting silane molecules at the silica surface leads to a reduction of the amplitude of the high-frequency silica process (process 1 in Figure 10), and to an increase in the corresponding activation energy. Accordingly, the presence of nonpolar molecules at the silica/polymer interface reduces both the amount of interfacial water molecules and their mobility. Interestingly, the activation energy of this process is an indicator of the strength of the NP-polymer interaction: 0.60 eV (57.9 kJ/mol) for bare silica, 0.65 eV (62.7 kJ/mol) for the same silica NPs modified with a coating agent, and 0.69 eV (66.6 kJ/mol) when a coupling agent is used. On the opposite, it was found that there is nearly no impact of the dispersion state that can be varied by reducing the mixing time on the dielectric relaxation of silica.

4.2 Structure-dependent charge migration in PNCs

The two different phases of nanocomposites – polymer and filler – are characterized by different electrical properties, and additionally interfacial polarization known as the Maxwell-Wagner-Sillars effect is generally present in PNCs, including filled rubbers [34, 41]. The MWS process arises from the migration of charge carriers present from the stage of mixing, such as additives or impurities, at

the filler/polymer interface. The trapped charge carriers form induced dipoles of large size leading to an additional contribution of the charges to ionic conductivity as illustrated in Figure 8. In this section, we review BDS results focusing on the interfacial polarization processes in PNCs with multi-scale filler structure. These processes as well as ionic conductivity are affected by structural reorganizations, which are themselves closely related to the mechanical properties [42, 43]. In other words, the microstructure, i.e., the nanoparticle dispersion, sets the frame for the dynamics. Consequently, the evolution of the BDS signal can be used to detect changes in the dispersion state.

4.2.1 Influence of water

A strong MWS polarization process has been reported in industrial rubber PNCs at the low-frequency side of the α-process (see Figure 8 for illustration) [35, 42, 44]. The position of this process within the experimental frequency window depends strongly on the water content – it becomes slower upon in-situ drying within the dielectric cell – whereas both its intensity and spectral shape are nearly unmodified [35]. The activation energy for this process is of the order of 0.55 eV (53 kJ/mol), also without any significant variation with the water content. The dielectric response of the MWS polarization has been described by the interlayer model (ILM) in SBR PNCs [35]. This model proposed by Steeman et al. [45, 46] considers a two-phase system with an adsorbed water layer located at the interface. As evidenced in Figure 11, the dielectric loss spectra at different hydration levels are well-reproduced by the ILM model using a single fit parameter, namely the water conductivity which depends on the water content and fixes the interfacial layer thickness. All these results indicate that MWS polarization in rubber PNCs is controlled by the amount of adsorbed water molecules at the silica surface, with a dielectric loss peak shifting reversibly within the frequency window.

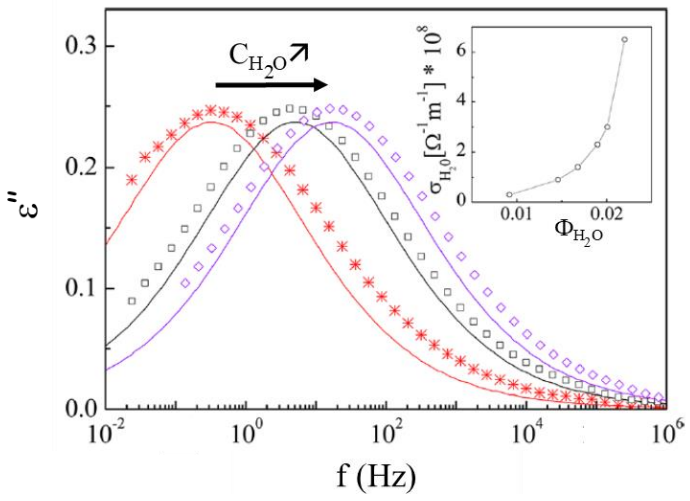

Fig. 11. Dielectric loss spectra at T = 295 K for SBR PNCs with 30 phr of silica and different water contents: C_{H2O} = 0.55%w (crosses), 0.95%w (squares), and 1.11%w (diamonds), after subtracting the α-relaxation and

conductivity contributions. Solid lines represent the ILM descriptions. Inset: interlayer conductivity σ_{H2O} as a function of water volume fraction Φ_{H2O}. Adapted from [35].

4.2.2 Evidence of filler percolation

Electrical conductivity has been used for a long time as an indicator of the formation of percolating paths of conductive filler in non-conducting matrices [47]. For example, the relationship between electrical conductance and dispersion in filled rubbers has been discussed for different NP types and shapes in a review article by M. Roland [48]. Here we choose to highlight original work by Le et al. on in-situ conductance measurements of SBR-carbon black PNCs [49]. A rather crude measurement of the dispersion by optical microscopy at selected moments during mixing gives access to the fraction of non-dispersed particle agglomerates bigger than a few microns, and thus to the inverse parameter termed "dispersion" in Figure 12. This parameter is found to increase with mixing time of the compounds, while the conductance varies in a non-monotoneous way. Its evolution has been separated in three stages by the authors: In the beginning, there is no infiltration of the CB by the polymer, and the electrical conductivity drops as the powder is incorporated. In stage 2 in Figure 12, the dispersion value increases strongly, and so does the conductance: the CB powder disperses while building up a network. In the last stage, finally, the best dispersion is obtained, corresponding to a break-up of any percolated network, and thus a slow decrease in conductivity.

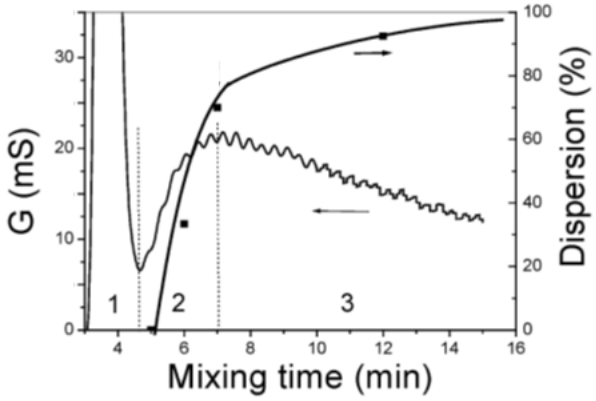

Fig. 12. Electrical conductance (left scale) measured in situ during mixing of 50 phr N220 carbon black in SBR; corresponding filler dispersion (right scale) measured at selected times is indicated by the symbols with a line as guide to the eye. Adapted from [49].

In the preceding section, we have seen that conductivity is not the only dynamical process sensitive to charge migration. Besides MWS1 denominating the process discussed in 4.2.1, a second interfacial polarization process labelled MWS2 has been evidenced by our group a few years ago in simplified rubber PNCs in the high-T range, well above the glass transition [42, 43]. The MWS2-process is located at the low-frequency side of MWS1 and its evolution with the silica content in PNC is shown in Figure 13a. It is visible at best for the lowest silica fraction with a broad dielectric loss peak in which two distinct contributions have been identified and described each by an HN function. For

higher silica contents, the peak overlaps with the strong contribution of ionic conductivity, but two processes are always necessary to describe the dielectric spectra quantitatively.

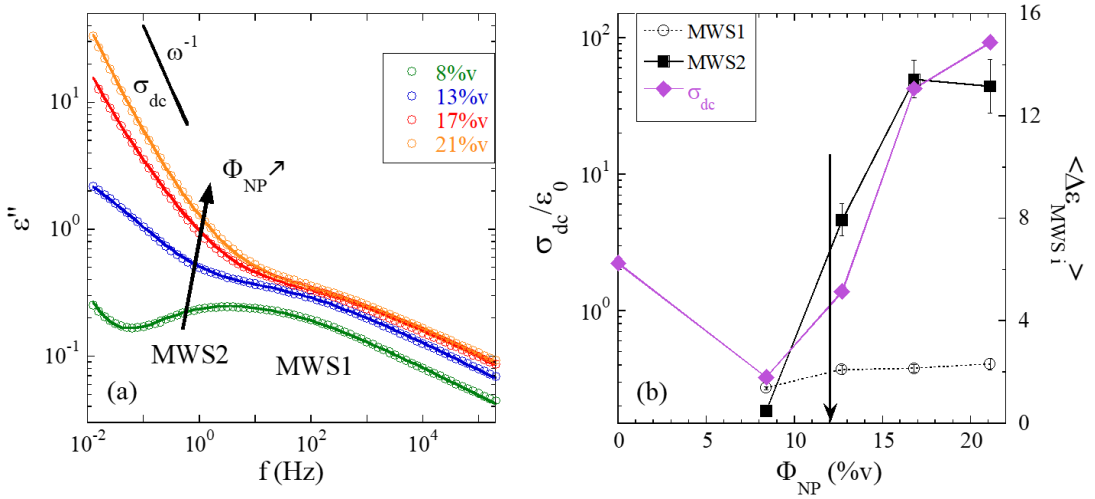

Fig. 13. a Dielectric loss spectra at 333 K for 50%F-SB PNCs with different Φ_{NP}. Solid lines are fits by the sum of two HN functions and a dc-conductivity term. **b** DC-conductivity at 393 K (diamonds) and average value of the dielectric strengths over T for MWS1 (circles) and MWS2 (squares) as a function of filler fraction for the same PNCs. The percolation threshold as obtained from rheology is indicated by an arrow. Adapted from [42].

For both MWS1- and MWS2-processes, the activation energies are found to be independent of the silica fraction. The activation energy of ca. 114 kJ/mol for MWS2 is similar to the one corresponding to the temperature dependence of the ionic conductivity. One may deduce that the dynamics of MWS2 is predominantly controlled by the polymer, as it was already the case for the ionic conductivity. On the other hand, the MWS2 time-scales are controlled by the filler concentration but not by the hydration level, indicating different origins for both interfacial polarization processes. Whereas MWS1 is a local phenomenon based on charge diffusion in water layers along the surface of silica aggregates (which are the building units of the microstructure, see section 3.2), the conduction mechanism of MWS2 consists of large-scale charge diffusion across the polymer matrix between aggregates. The evolution of the dielectric strengths of both MWS1 and MWS2 processes as a function of the silica fraction is reported in Figure 13b together with the ionic conductivity. The latter exhibits first a decrease attributed to the reduction of free charges in the polymer matrix due to trapping at the silica surface. It is followed by a two-order of magnitude increase in the range of the percolation threshold as determined independently by means of rheology on the same samples. Here it is found that MWS1 depends only marginally on the silica content and thus microstructure, whereas MWS2 is strongly impacted by large-scale structural reorganizations with the formation of a percolated network of aggregates. One may note here that a similar process to MWS2 has been partially identified in carbon black filled rubbers and linked to structural reorganization due to crosslinking or high-temperature treatments [50]. In these experiments, flocculation in SB-carbon black PNCs just below the percolation threshold has been induced by thermal treatments. The effect could be followed via the

increase in mechanical strength, with the simultaneous development of a Payne effect indicative of filler networking. In parallel, BDS measurements have been interpreted in terms of charge migration across gaps between filler NPs, and closing of these gaps is consistent with the formation of filler networks. Innovative experiments coupling *simultaneous* dielectric and mechanical spectroscopy have been reported by Huang et al. in NR-carbon black PNCs [47]. These authors link the modification of interfacial polarization to mechanical properties. In PNCs of high filler content, a significant decrease of the real part of the permittivity under increasing strain is concomitant to the classical Payne effect on G'. A similar confrontation with mechanics has been followed by us in an above-mentioned article [26], however without details on charge migration by BDS measurements indicative of filler contact. Scattering and mechanical Payne-effect experiments show that thermal treatment may be used to rejuvenate a flocculated and possibly percolated aggregate structure, after having destroyed the filler network by milling.

It is thus possible to connect the dynamical dielectric response of these interfacial processes with the various structural length scales. Such an approach is original as BDS is not a spatially-resolved experimental technique, which is why it is only rarely used [47, 51] to access structural information, beyond simple conductivity measurements. The latter are a common approach to the detection of percolation since the invention of the carbon microphone some 140 years ago.

4.2.3 Impact of grafting density

As described in section 3.2, the use of graftable polymer chains is a powerful way of controlling the dispersion state which sets the frame for the mechanical properties of rubber PNCs. The dielectric response of a series of simplified nanocomposites with different amount of functionalized SB chains is illustrated in Figure 14a. The strong evolution of the dielectric loss with grafting is clearly visible, and the decomposition into the above-mentioned interfacial processes, MWS1 and MWS2, is also shown.

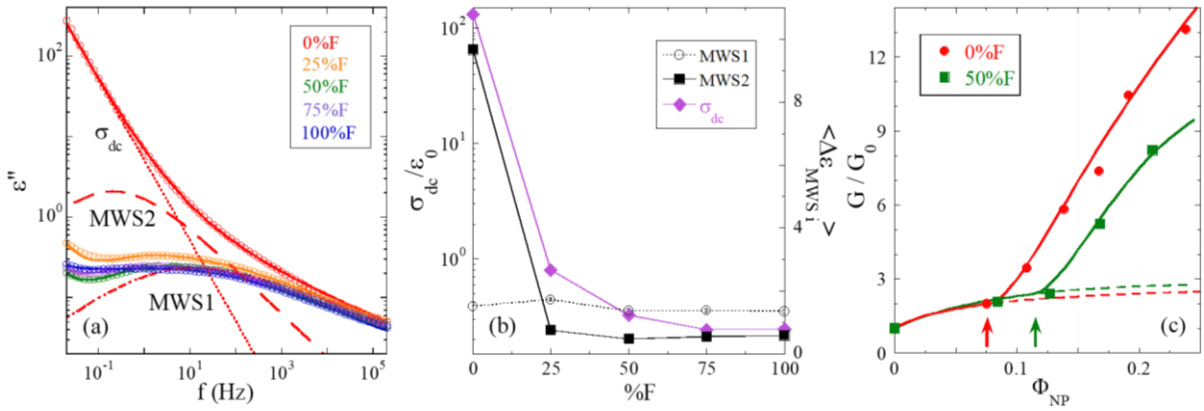

Fig. 14. a Dielectric loss spectra at 333 K for SB PNCs with ca. 8.5%v of silica and different amounts of graftable chains. Solid lines are fits by the sum of two HN functions and a dc-conductivity term. Individual contributions are included for the sample without graftable chains. **b** DC-conductivity at 393 K (diamonds) and average value of the dielectric strengths over T for MWS1 (circles) and MWS2 (squares) as a function of matrix composition for the same PNCs. **c** Rheological response at 60 Hz in terms of the reinforcement factor G/G_0 as a function of silica fraction for SB PNCs with 0%F (circles) and 50%F (squares). Solid lines are fits discussed in [12], arrows indicate the percolation threshold. The purely hydrodynamic reinforcement, $1+2.5\Phi_{agg}$, is also included (dashed lines). Adapted from [43].

The evolution of the dielectric strengths as well as the ionic conductivity is reported as a function of the fraction of graftable chains in Figure 14b in analogy to Figure 13b. The strength of the local MWS1 process is mostly unaffected by grafting whereas the MWS2 strength is found to follow the same evolution as the ionic conductivity, as already observed in Figure 13b. Here, a significant drop of the MWS2 intensity at ca. 25% of functionalized chains is observed, which is interpreted as the break-up of the percolated aggregate network upon grafting at fixed silica content. This effect has been termed depercolation. It is directly related to the evolution of the filler structure with polymer grafting (section 3.2). The formation of aggregates of lower mass at low grafting density notably shifts the mechanical percolation threshold as evidenced in Figure 14c. There, the reinforcement factor defined as the ratio of the plateau moduli of PNC and pure matrix is plotted as a function of the filler fraction for different grafting densities. These data have been fitted using a percolation model based on percolating aggregates within large-scale branches extending across the sample. It uses the aggregate volume fraction deduced from the combination of SAXS and TEM as main variable instead of the silica fraction. The good description of the rheological data in Figure 14c underlines the consistency of the proposed approach. Moreover, the volume fraction at percolation, and its shift with functionalization, agrees nicely with the dielectric analysis of interfacial processes. Following the evolution of such processes is thus a sensitive tool to probe large-scale structural reorganization in rubber PNCs.

4.3 Segmental dynamics of rubber compounds

The segmental relaxation of polymer matrices is the physical origin of dominating macroscopic rheological properties crucial for industrial applications. There is a large body of results related to fine-tuning these properties, and following our industrial application of car tire treads we review here only effects of crosslinking-related additives (in particular activators), as well as blends, with dielectric spectroscopy as main technique. Once the matrix-only part is understood, we will turn to polymer nanocomposites, with a critical discussion of the modification of the segmental dynamics close to nanoparticle interfaces in weakly interacting rubber systems like SBR-silica. Here BDS is complicated to analyze due to overlapping processes, and some recent neutron scattering results are discussed.

4.3.1 Unfilled rubbers: vulcanization and miscible rubber blends studied by BDS

4.3.1.a Following vulcanization mechanisms by dielectric spectroscopy

The vulcanization of rubber leading to the formation of a permanent 3D-network is required to enhance the macroscopic properties of the final product. This process involves a large number of additives beyond sulfur (e.g., ZnO, stearic acids, CBS, among others listed in Table 1), which makes it rather complex due to possible interactions between the different additives and also interactions with the silica filler. All additives are present in the formulation in small quantities with respect to the polymer (typically between 1 and 5 phr each) and quite a few of them possess a strong dipole moment (e.g., 2.90 D for CBS, 3.99 D for DPG) [52, 53]. It follows that a sensitive and selective technique as dielectric spectroscopy is a highly appropriate tool to study the impact of the presence of vulcanization additives on the segmental relaxation. Modifications of the dynamics that are observed by BDS may be helpful for a better understanding of the vulcanization mechanism, which is critical for technological developments. These effects are reviewed here for unfilled rubber.

Ortiz-Serna et al. report dielectric measurements carried out on samples of natural rubber containing the common vulcanization additives but processed to avoid vulcanization [54]. The dielectric spectra reveal a broad loss peak that could be described by two contributions: a fast α-process due to the segmental motions of NR, and a slower process assigned to the dynamics of stearic acids linked to the NR chains. The authors studied the impact of water and found, surprisingly, that the dielectric strength of the low-frequency contribution is higher for the dry rubber. This effect is interpreted as a consequence of different ordering of the lipid hydrocarbon chains which depends on the water content. High pressure dielectric spectroscopy was also used to track the influence of temperature and density on the segmental dynamics. It shows that the relaxation processes detected here are driven by temperature variation instead of free volume. In a similar NR-based system, Hernandez et al. also report a second relaxation process, slower than the segmental dynamics of NR [55]. Going through a step-by-step study where the different vulcanizing additives are removed one by one, they rather

attributed the slow process to ionic clusters of ZnO. These clusters act as crosslink precursors, which restrict the mobility of interfacial polymer segments, confirming the role of ZnO as activator for sulfur vulcanization. This result is in agreement with a previous SANS study on vulcanized polyisoprene (the synthetic version of NR) swollen in a deuterated solvent [56]. The SANS results evidenced heterogeneous network structures formed by high-density network domains which surround ZnO clusters dispersed in the rubbery matrix. Stearic acids are nonetheless necessary to disperse ZnO and form zinc stearate after reaction, promoting crosslinking.

In the same spirit as Hernandez et al. [55], the effect of vulcanizing agents in unfilled SBR mixtures has been explored by Ortega et al. [52]. The same kind of slow contribution to the α-relaxation peak has been observed by BDS and it is evidenced in Figure 15a. By comparing the dielectric response of the mixture without one or the other additives, the slow process could be assigned to the cure accelerator couple, DPG and CBS (see Figure 15b). Furthermore, there is a dominant effect of the DPG content on the dielectric strength of this process. It was also demonstrated that DPG itself (and not byproducts from the vulcanization reaction) is related to the slow process by comparing the dielectric response of a sample before and after in-situ vulcanization in the dielectric cell. BDS measurements under pressure showed that both contributions to the α-process display a similar activation volume (same shift of the relaxation times with pressure), indicating that the dynamics of DPG is coupled to the segmental dynamics. The latter is itself not modified by the presence of DPG. Lindemann et al. determined an activation energy of ca. 150 kJ/mol for the slow process in the same SBR system showing that it may eventually merge with the segmental relaxation in the high-temperature range [57]. Looking finally to the filled rubber mixture [52], the slow process is found to display a lower dielectric strength in presence of silica presumably due to the lower amount of DPG available in the matrix as this molecule tends to adsorb on the silica surface.

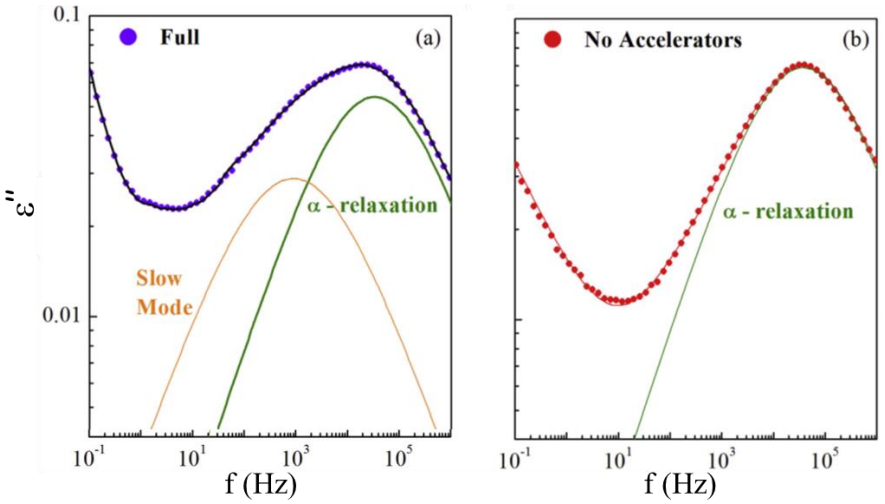

Fig. 15. Dielectric loss spectra at T = 289 K for F-SBR. **a** Full formulation, **b** the same formulation without DPG and CBS accelerators. Solid lines represent the fits to the experimental data using one or two Cole-Cole functions (δ = 1 in Eq. (3)) and a conductivity term. A single relaxation is observed in **b**. For the sake of clarity, the conductivity contribution is not shown. Adapted from [52].

The examples discussed above highlight that a slower contribution to the segmental dynamics is systematically observed in rubber systems containing vulcanizing additives. This contribution may have different molecular origins depending on the polymer and the set of additives present in the recipe.

4.3.1.b Studying miscible rubber blends by dielectric spectroscopy

The dynamical properties of thermodynamically miscible polymer blends – even in absence of filler NPs – represent an entire research topic of their own [58]. This is due to the possibly wide dynamical asymmetry, where the interplay of the segmental dynamics of each compound can induce qualitatively new phenomena. Dynamical asymmetry refers to the fact that the α-relaxation of each polymer may be active at very different frequencies – or in other words, they display a large difference in individual T_g's. A representative example of asymmetric blends is the well-known poly(ethylene oxide)/poly(methyl methacrylate) blend [59]. Following the literature and in particular the groundbreaking work of the groups in San Sebastian [58] and Jülich, [59, 60] uncrosslinked blends usually show a common, intermediate macroscopic (calorimetric) T_g. If one resolves selectively the segmental dynamics with BDS, the surprising finding is that two distinct processes corresponding to the segmental dynamics of each component are reported with slight modifications due to the local composition in the blend. A rationalization of this effect based on the concept of self-concentration linked to chain connectivity has been proposed by Lodge and McLeish [61]. It was further refined by combining this concept with the Adam-Gibbs theory [62] linking structural relaxation time and configurational entropy [63]. If, however, one forces the interaction between the two chains by

introducing specific connections (hydrogen bonds or crosslinks), then the local processes average out to a single one, i.e., dynamic heterogeneity may not persist on the probed length scale.

The segmental dynamics of vulcanized SBR/BR blends prepared by solid-phase mixing has been investigated recently. These are two miscible polymers, which are both dielectrically active, with a large difference in T_g of about 80 K. In this industrially relevant system, a single loss peak has been reported by BDS for the α-relaxation, indicating the same – or at least close – segmental relaxation times for the two polymers. In a recent contribution by the group of Blume, Rathi et al. [64] focus on the distribution and impact of extender oils (TDAE) on mechanical performance of tire treads, namely wet-skid resistance, low wear, and low rolling resistance. These properties are difficult to predict presumably due to dynamical heterogeneities within the blend. They observe a systematic broadening of the glass transition in 50/50 vulcanized blends studied by calorimetry, dynamic mechanical analysis, and BDS. In dielectric spectroscopy, the authors decompose the single loss peak of the blend without TDAE (see Figure 16) into a fast α and a slow α_0 process, each described by an HN function: the fast α-process is associated with the contribution of dissociated polybutadiene segments, while the blended SBR and polybutadiene segments lead to the slower α_0 process. For the blends with extender oil, the general trend is that both the α and α_0 processes show longer relaxation times with increasing amounts of oil, which was to be expected since the TDAE oil has slower relaxation dynamics compared to the blends. However, there is a larger effect on the fast α-relaxation coming from polybutadiene segments only, which is similar to the effect of the oil on pure BR. The dynamical heterogeneity is thus reinforced by the presence of the oil, contributing to the complex material response.

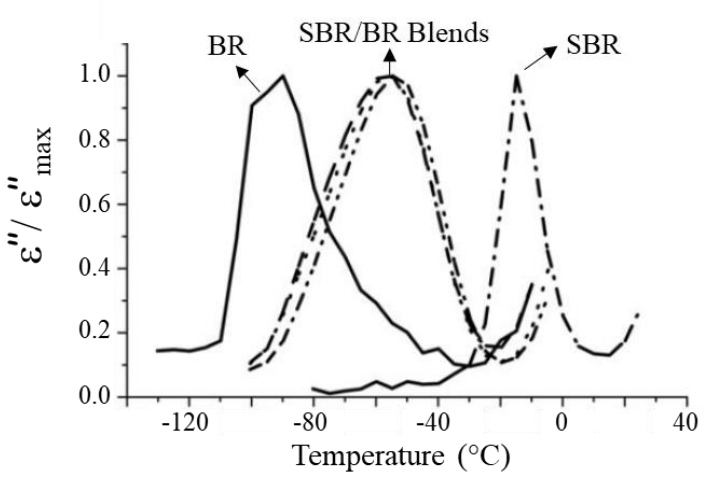

Fig. 16. Dielectric loss spectra normalized to their maxima versus temperature at 1 Hz for pure polymers: SBR and BR, and for the SBR/BR blends with different contents of TDAE oil : — — 0, - - 10, and − - 20 phr. Adapted from [64].

Starting from the individual components – BR and SBR of different microstructure –, Schwartz et al. in collaboration with Goodyear quantitatively describe dielectric spectroscopy results of the vulcanized blends with a modified Adam-Gibbs approach [36]. The latter relates the time scale of the segmental motion to the excess entropy of the mixture taking into account the interactions between components via an effective Flory-parameter, χ_{eff}. As outlined above, a single segmental relaxation process is observed due to the strong intermolecular interaction provided by the crosslinks, and the temperature dependence of the relaxation times is well-described using the proposed model. The resulting interaction parameter quantifies the T-dependent change in configurational entropy, and it can even be negative (lower entropy) for unfilled blends at the highest temperature, presumably implying a more efficient packing. The interaction is moreover shifted with the chain composition, and also with silica-filling, using precipitated silica at a rather high load (120 phr). The model thus accounts for the presence of the filler NPs in terms of an increased interaction between chains.

4.3.2 The complex analysis of the dynamics of filled rubber: dielectric *vs.* neutron spectroscopy

The segmental dynamics of SBR loaded with silica filler has attracted considerable attention over the past two decades. The question of modifications of the polymer dynamics close to the interface has been approached with various techniques, in particular mechanical measurements [65-68], and of course BDS [40, 69, 70]. The problem which has triggered considerable discussion in the literature is that most of these results – however well done on each specific system and for each experimental approach – are not mutually consistent: sometimes an interfacial layer of slowed down dynamics is reported, and sometimes there is basically no impact of the presence of silica on the segmental dynamics. Depending on what one wishes to promote, authors thus have the natural tendency to cite either one or the other of these "schools"… It is not the purpose of this modest chapter to review this entire discussion, but we attempt to replace some studies in this context. First of all, Arrighi et al. have shown the existence of a second high-temperature contribution in mechanical measurements of crosslinked SBR-silica systems represented as the loss tangent, tan(δ), *vs.* temperature [65]. This additional process is enhanced by the addition of a coupling agent and it is attributed to a dynamical change in a nanometer-thick interface, assuming a given filler structure. The second tan(δ) peak in the viscoelastic response of SBR PNCs is also reported by Tsagaropoulos and Eisenberg [66] whereas it is not visible in the data of Mélé et al. [67] and Robertson et al. [68], though in both cases notable differences on the high-temperature side of the tan(δ) peak are observed. It has been pointed out by Robertson et al. that the observed differences in tan(δ) do not necessarily reflect modifications in the segmental dynamics of the polymer as the loss modulus is essentially not evolving with the polymer-filler interaction. They may rather be due to filler-network contributions and the variation of the elastic modulus (reinforcement), or restricted terminal flow in presence of NPs [71, 72]. It is thus not always necessary to invoke mobility-restricted polymer layers near the filler nanoparticles. The same SBR-

silica system [65] has been studied by BDS by Pissis et al. [69], and they speculate on the influence of the surface treatment on structure – without having access to quantitative measurements –, and finally on MWS processes that are more pronounced when untreated silica is used possibly due to aggregate formation. Fragiadakis et al. propose work on natural rubber filled with in-situ created silica [70]. Two states of dispersion have been prepared, unfortunately again without any quantitative characterization, and these authors could show that only the better dispersion leads to a small increase of the calorimetric T_g, with a silica-dependent low-frequency process observed at 2 to 3 orders of magnitude below the main α-relaxation. Such a strong effect – with a restricted mobility extending over a ca. 3 nm-thick interfacial layer – is difficult to understand taking into account the weak interaction between NR and silica, and may result from very specific sample preparation. From these different examples, it is clear that the following points deserve further attention:

a) System preparation: any small surface-active molecule (e.g., coating agents) may also influence dynamical matrix properties, and thus also rheology. Complex systems are thus … complex to analyze.

b) Robustness of the interpretation of complex BDS spectra: given the very broad range of most dielectric processes, it is not easy to discard the influence of other processes on the position and shape of a given one (like MWS on the segmental relaxation).

c) Crosscheck by other techniques: which other microscopic probe can be used to analyze local polymer dynamics?

d) Microstructure: knowledge of the primary NP size is important, but not always sufficient to characterize the amount of polymer in interaction with filler structures. What about aggregation states, and interlayer overlap?

In reply to these points, we have designed the simplified-industrial system defined in section 2. Moreover, the adsorption isotherm of coating agents on filler NPs has been investigated in-situ and is discussed below. This work illustrates the differences between system design (all molecules should go to the interface), and reality (some do not!). Next, the overlap with MWS-processes which have been detailed in the above subsection may, or may not, influence the shape of the α-relaxation process. Without a quantitative description of the latter, it is difficult to conclude on either a shift, a broadening, or the generation of an additional process for the segmental motions. As observed already by Meier et al., a broadening (without shift) of the dielectric loss peak with increasing silica content seems to be robust [40] – these authors do not identify any strong MWS process which could alter the interpretation, but this may be structure and loading dependent. The broadening is presumably related to the slowed-down dynamics of the chain molecules close to the interface, but the authors do not provide a detailed analysis of the α-relaxation and focus, as mentioned above, on the secondary relaxations. On the other hand, nano-dielectric measurements based on an AFM-type apparatus have shown that there is no detectable change in local dynamics across a sample, regardless of the distance

to the next filler surface [73]. Despite locally different mechanical properties defining an interacting layer, the observation of bulk-like segmental dynamics in this layer may result from the use of a coupling agent acting as flexible link between the polymer and the silica filler.

The question of cross-checking BDS results, in particular if peaks are ill-resolved, brought us to QENS outlined briefly below. These results clearly show that the change in dynamics in weakly interacting rubber systems is systematically present, but equally systematically small. Of course, structural investigations range also under "additional techniques", which is why we have opened the present chapter with a detailed review of recent advances in this field. If one focuses, e.g., on the thickness of the interfacial layer, the latter is usually deduced from some overall fraction of dynamically-modified polymer. As a function of the filler landscape onto which this 'slowed-down' volume is distributed, different thicknesses are obtained: thus the thickness of the interfacial layer depends in a crucial way not only on particle size, but also on dispersion. As an example, Papon et al. have tackled this problem in silica-acrylate PNCs [74], making use of a RMC approach as described in section 3.4. The result is a statistical representation of overlapping interfacial layers, which is related to the degree of vicinity, i.e. positional correlation, of the nanoparticles. Close-by NPs thus share interfacial layer, thereby increasing their thickness with respect to the ideal, fully dispersed system having the same amount of slowed-down volume.

4.3.2.a Dielectric and neutron spin-echo spectroscopy applied to simplified industrial systems

Figure 17a shows the dielectric data of a simplified SB PNC containing 20%v of silica. The dielectric loss exhibits a strong MWS contribution with a poorly-defined high-frequency shoulder associated with the α-relaxation. The data in Figure 17a have been described using the sum of two HN functions plus a purely dc-conductivity term. For consistency with the following QENS data, where a stretched exponential function – known by the names of Kohlrausch, Williams and Watts (KWW) – is used to describe the relaxation behavior in the time domain, we used coupled shape parameters in Eq. (3) to describe the α-process, following the connection between the frequency-domain HN function and the KWW function proposed by Alvarez et al. [75, 76]. It is clear from Figure 17a that there are large uncertainties regarding the shape and position of the α-process. Indeed, an equivalently good description of the data is obtained using a selection of stretching exponents β ranging from 0.44 (the value obtained for neat SB) and 0.30. The corresponding – compatible – distributions of relaxation times for the segmental dynamics in PNC are thus possibly larger in presence of silica, as illustrated in the inset of Figure 17a. Interestingly, the representative average characteristic times, $\langle\tau\rangle = \tau_W \Gamma(1/\beta) / \beta$, associated with these functions still lies in a very restricted range (-4.2 to -4.4 in log scale, including the pure matrix timescale), in agreement with the observation of a constant calorimetric T_g. Such results indicate that the segmental dynamics is only weakly affected by the presence of silica in the

rubber system. This was confirmed by low-field NMR measurements on similar simplified samples [43], but also on their vulcanized counterparts including the whole ingredient list [77]. In both cases, the fraction of rigid polymer amounts only to a few percent, i.e., much lower than values reported for colloidal silica NPs dispersed in poly(ethyl acrylate) using either a coating or a coupling agent [78]. The small rigid fraction detected by NMR has nevertheless a critical role in the viscoelastic response of filled rubbers [77].

Here, one may wonder about the dynamical response of colloidal nanocomposites based on the same SB polymer as used in the simplified industrial formulation but incorporating well-defined spherical NPs (see the model system defined in section 2). In this case, the dispersion state as discussed in section 3.4 is rather good, without the typical multi-scale structure of industrial PNCs which involves strongly interacting aggregates. Accordingly, one can see in Figure 17b that the MWS process is less intense and shifted towards lower frequency. As a consequence, the α-process is now well-defined in the frequency window probed by BDS and its description points towards a broader distribution of relaxation times (β = 0.35, see inset in Figure 17a) with respect to the neat polymer. The position of the maximum of the distribution is not modified by the presence of silica, and only a negligible slowing down of the average characteristic times (log ⟨τ⟩ = - 4.1) is observed. There is thus a minor impact of the silica NPs on the segmental dynamics in the model PNC in spite of a larger range in relaxation times.

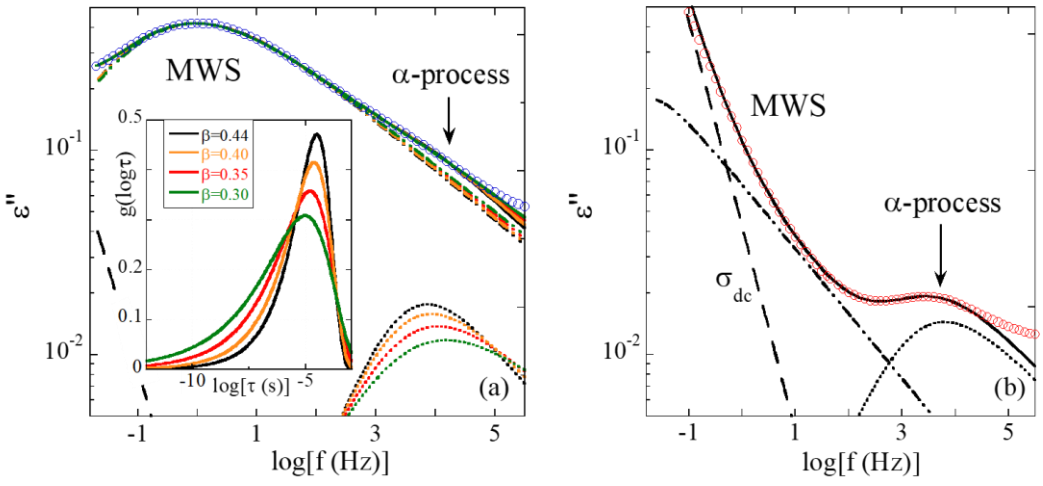

Fig. 17. Dielectric loss spectra of SB PNCs with ca. 20%v silica at T = 273 K. Lines are fits by a purely dissipative dc-conductivity term (dashed line) and two HN functions: interfacial MWS process (dashed-dotted lines) and α-process (dotted lines). **a** Simplified-industrial PNC. Four different spectral shapes associated with the KWW distributions given in the inset are shown to reproduce the α-process. β = 0.44 corresponds to the stretching exponent obtained for the pure SB matrix (black curve). **b** Colloidal PNC. The KWW distribution of relaxation times associated with the α-process in this model PNC is given in the inset (red curve, β = 0.35).

Given the impossibility to correctly resolve the α-relaxation in industrially-simplified PNCs, QENS has been employed in a recent study [32]. Due to their rather low energy, which unlike the one of X-ray photons is comparable to k_BT, neutrons are often the only radiation probe capable of investigating spatially resolved dynamics. Neutron spin echo spectroscopy (NSE) is one of these methods. It is based on the measurement of the changes in neutron speed after interacting with the sample. It is usually performed with deuterated samples (coherent scattering) in order to study the collective motions associated with the segmental relaxation, but this is difficult here for practical reasons, in particular cost issues for large samples. NSE can also be used with hydrogenated samples to probe incoherent scattering, though the signal is strongly reduced in this case [79]. In our study, we have chosen the relevant q-range in order to avoid coherent scattering of the filler. We have then been able to demonstrate that incoherent NSE can be used to access small changes of segmental dynamics of simplified-industrial PNCs. The self-dynamics of the polymer chains in presence of the filler is shown in Figure 18a where it is compared to the neat polymer. Due to the chosen q-vector, the spatial scale of these modifications is approximately 1 nm, and as they are caused by the NPs, they thus must take place close to the filler interface. As a result, our high resolution NSE-measurements show for the first time that the segmental motion is slightly but systematically slowed down by the presence of the industrial filler NPs, without modification of the width of the time distribution in the high T-range well above T_g. Moreover, this is observed at all temperatures studied here (100°C to 160°C), and these results could be superimposed to the relaxation map in Figure 18b. The NSE-relaxation times are in the continuation of the dielectric ones of both model and industrial systems, in a domain inaccessible for BDS as discussed above. They show that even in strongly aggregated system, the shift in relaxation time is small – but nonetheless always present at high T.

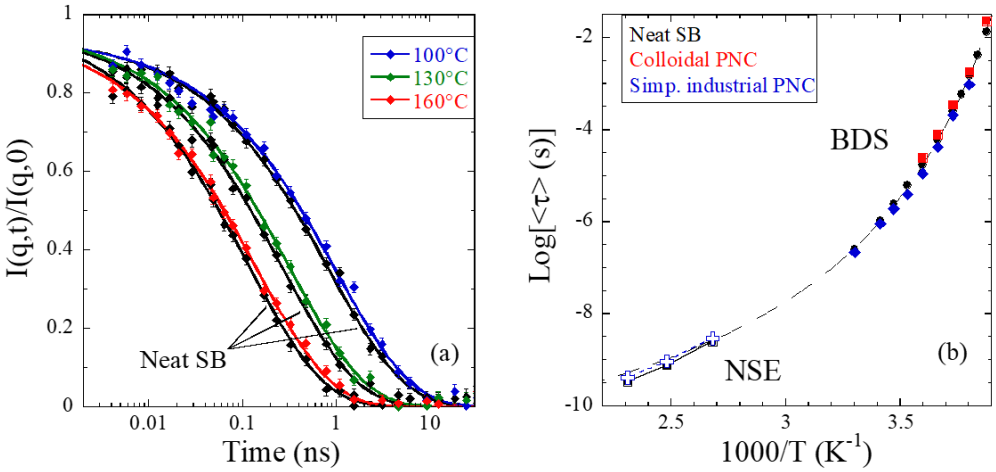

Fig. 18. a NSE data at q = 0.54 Å^{-1} for the neat SB (black) and the simplified-industrial SB PNC with 20%v of silica measured at different temperatures. Lines are fits using a KWW function with β = 0.55. **b** Relaxation map with the characteristic average times for segmental relaxation from NSE data (q = 0.54 Å^{-1}) and BDS for the simplified-industrial and colloidal PNCs (same filler content) and the pure SB polymer. For the industrial PNC, the same shape parameter as for the matrix has been used in the analysis of the BDS spectra for consistency with NSE. The Vogel-Fulcher-Tammann (VFT) fit of the BDS times for the pure polymer matrix is represented by a dashed line. Adapted from [32].

4.3.2.b Studying in-situ adsorption of small molecules onto filler particles by dielectric spectroscopy

We have seen in section 4.3.1 that additives to the polymer matrix possibly modify their dynamical properties, and that this can be probed by BDS. In a recent approach, we have made use of this effect in order to study the partition of silane coating molecules between the silica filler and the SB polymer matrix in a model PNC [80]. The idea behind this is that coating agents are part of the standard formulations of industrial PNCs, but it is difficult to know if they really go only to the filler interface. As we have seen in the NSE-section above, it is challenging to isolate by BDS the segmental relaxation signal in the more complex industrial PNCs, and therefore we have chosen to investigate the model system. Using the plasticization effect of the coating agents blended with the unfilled SB polymer, we have first established a BDS-calibration curve shown in Figure 19a. This calibration is based on the shift of the α-process towards higher frequency when increasing the amount of coating agent in the unfilled matrix. In presence of silica in a PNC sample without grafting of the silanes, i.e., where silanes are free to go either in the bulk or at the silica surface, it is thus possible to determine the mass fraction of coating agent dispersed in the matrix, ζ_{free}, via its impact on the position of the dielectric loss peak. Then, by mass conservation one can conclude on the quantity of coating agent actually covering the silica surface by adsorption. In Figure 19b, the dielectric response for PNC-systems is shown for different options of activation of grafting of the coating agents in PNCs. They are compared to the neat polymer (without any NPs) in presence or absence of coating agent. The result is that the loss peak for a PNC without grafting of the silanes is located in between those of the pure SB matrix blended with an equivalent amount of silanes and the same PNC where grafting has been activated (i.e., no free silane in the bulk). This demonstrates partitioning of the coating agent between the functionalized matrix (via chemical compatibility) and the NP interfaces. A similar phenomenon is expected in industrial rubber PNCs in the first stage of mixing, before grafting reactions are activated. As a final result, we have determined the adsorption isotherm of the coating agent onto the filler within the PNC (not shown, [80]). The isotherm tells us that the maximum adsorbable amount is reached for the lowest silane concentration used in formulations, which also corresponds to industrial standards. It is concluded that this concentration must have resulted from an optimization of properties of the nanocomposites while using only a minimal amount of agents.

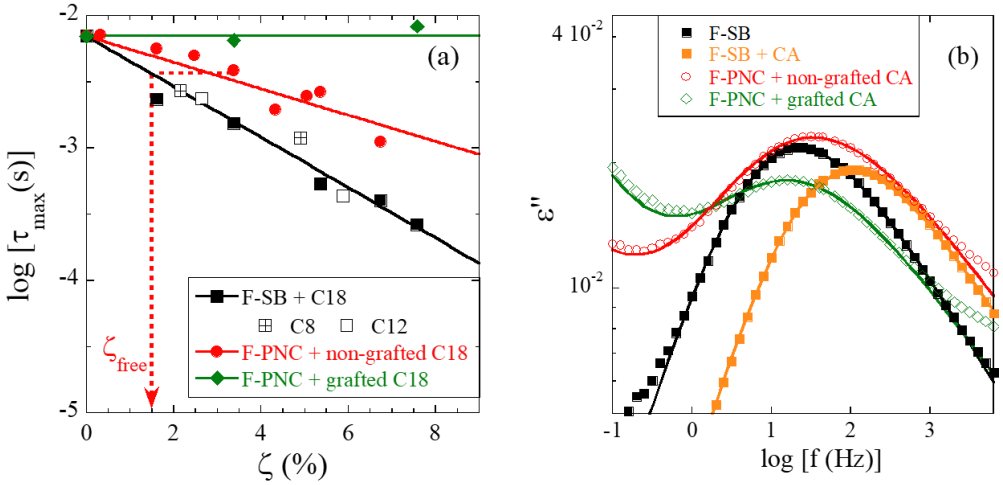

Fig. 19. a BDS segmental relaxation time at T = 258 K as a function of the nominal silane matrix concentration ζ in F-SB. Calibration curve for polymer with various amounts of silane, C_8 (crossed empty squares), C_{12} (empty squares) and C_{18} (plain squares), in F-SB. The solid black line represents a linear fit to all silanes in log-representation. The data for PNCs without (resp. with) activation of the grafting reaction are superimposed (red circles, resp. green diamonds) for nominal ζ in samples, together with a linear fit for the non-grafted PNCs. The construction (red dotted lines) illustrates the determination of the effective ζ_{free} within the matrix in presence of NPs. **b** Dielectric loss spectra at T = 258 K of F-SB (without and with C_{18} at ζ = 3.4%) and F-PNCs ($\Phi_{NP} \approx$ 10%v, same amount of C_{18}). Possible silane grafting is indicated in the legend. Solid lines represent the fit to the experimental data based on Eq. (3) plus a purely dissipative dc-conductivity term. Adapted from [80].

5. Conclusion

We have reviewed recent studies of the filler structure and the polymer dynamics of nanocomposites of industrial relevance, including segmental relaxation and interfacial polarization processes at the polymer-nanoparticle interface. Structural studies have been shown to have progressed to a large extent through the quantitative analysis of the small-angle scattering, even for complex industrial filler nanoparticles with multi-scale structure. Interfacial polarization processes are not always visible in dielectric spectroscopy, as they depend on the large-scale filler structure of the samples (MWS2) or the water content (MWS1), and thus on details of formulation. If MWS-processes are dominant, which is typically the case for large filler assemblies or percolating networks, they may impact the analysis of segmental dynamics. While there has been a lively discussion in the literature about the effect of nanoparticle interfaces on the segmental dynamics of the polymer in close vicinity, we have chosen to broaden the view and include the effect of additives, and blending. In presence of nanoparticles, several recent contributions including nano-dielectric measurements and neutron spin echo spectroscopy seem to indicate that the modification of the dynamical response of the polymer is only weakly affected in rubbery systems, in particular silica-SBR: in such elastomeric systems of weak polymer-particle interaction, there is a small but nonetheless detectable shift of the whole relaxation time distribution of segmental dynamics in the high-T range, in agreement with NMR studies. Our understanding of the weak interfacial layer in silica-based rubber system has thus made a few steps

forward after patiently seeking and assembling information on the microstructure of such systems, characterizing the influence of additives, and finally focusing on segmental dynamics with combinations of dielectric and neutron scattering techniques. Weakly interacting rubber PNCs may be opposed to systems with strong attraction like poly(2-vinyl pyridine) (P2VP) mixed with silica – reviewed by key players in the field in this collection [81]. In such systems, a distinct interfacial mobility extending over several nanometers is resolved by BDS. This second process is attributed to the slowed-down dynamics of the interfacial layer, and it shows a peculiar chain-mass dependence, which suggests that it is related to chain packing properties close to the interface [82]. On the other hand, bulk mobility is found not to be impacted. Interestingly, a measurable static interfacial layer formed by out-of-equilibrium chain packing leading to a lower density could be evidenced by SAXS [83]. It is tempting to identify the static and the dynamic interfacial layers in attractive PNCs, but many more questions need to be addressed beforehand: while the spatial extension of both layers is in the nanometer range, it is unclear why the decrease in local density as described by reverse Monte Carlo is accompanied by a slowing-down of this layer. In this context, the idea of chain stretching in the interfacial region has been put forward [81]. It is also consistent with measurable enhancement of mechanical moduli in the interfacial layer even in the glassy state. A balance between chain stretching and density variations may thus control the interfacial layer properties. There remain thus many open questions to be answered in the field of glassy or rubbery polymer nanocomposites, and it is concluded that the field of segmental dynamics in complex polymer-nanoparticle systems will stay a fascinating challenge for yet some years to come.

Acknowledgements. Access to experimental installations and chemicals by Michelin, Solvay and Synthos is gratefully acknowledged. Support by the European Soft Matter Infrastructure (EUSMI) for conducting the BDS experiments in San Sebastian is highly appreciated. Scattering experiments would not have been possible without powerful beamlines and support at large-scale facilities (ESRF, ILL and Soleil).

References

1. Jancar J, Douglas JF, Starr FW, Kumar SK, Cassagnau P, Lesser AJ, Sternstein SS, Buehler MJ (2010) Polymer 51:3321-3343
2. Heinrich G, Klüppel M, Vilgis TA (2002) Curr Opin Solid State Mater Sci 6:195-203
3. Chazeau L, Brown JD, Yanyo LC, Sternstein SS (2000) Polymer Composites 21:202-222
4. Payne AR (1962) J. Appl. Polym. Sci. 6:57-63
5. Mark JE, Erman B, Eirich FR, *Science and Technology of Rubber*. Academic Press: San Diego, 1994.

6. Banc A, Genix AC, Dupas C, Sztucki M, Schweins R, Appavou MS, Oberdisse J (2015) Macromolecules 48:6596–6605
7. Glomann T, Schneider GJ, Allgaier J, Radulescu A, Lohstroh W, Farago B, Richter D (2013) Phys Rev Lett 110:178001
8. Papon A, Montes H, Hanafi M, Lequeux F, Guy L, Saalwächter K (2012) Phys Rev Lett 108:065702
9. Stephen R, Thomas S, *Rubber Nanocomposites: Preparation, Properties, and Applications*. Wiley: 2010.
10. Wolff S (1996) Rubber Chem. Technol. 69:325-346
11. Musino D, Genix A-C, Fayolle C, Papon A, Guy L, Meissner N, Kozak R, Weda P, Bizien T, Chaussée T, Oberdisse J (2017) Macromolecules 50:5138-5145
12. Baeza GP, Genix AC, Degrandcourt C, Petitjean L, Gummel J, Couty M, Oberdisse J (2013) Macromolecules 46:317-329
13. Genix AC, Baeza GP, Oberdisse J (2016) Eur. Polym. J. 85:605-619
14. Guy L, Daudey S, Bomal Y (2009) Kautschuk Gummi Kunststoffe 62:383-391
15. Baeza GP, Genix A-C, Paupy-Peyronnet N, Degrandcourt C, Couty M, Oberdisse J (2016) Farad. Discuss. 186:295-309
16. Baeza GP, Genix AC, Degrandcourt C, Petitjean L, Gummel J, Schweins R, Couty M, Oberdisse J (2013) Macromolecules 46:6388–6394
17. Baeza GP, Genix AC, Degrandcourt C, Gummel J, Couty M, Oberdisse J (2014) Soft Matter 10:6686–6695
18. Genix A-C, Oberdisse J (2017) Soft Matter 13:8144-8155
19. Larsen AH, Pedersen JS, Arleth L (2020) J. Appl. Cryst. 53:991-1005
20. Beaucage G, In *Polymer Science: A Comprehensive Reference*, Möller, M. a., Ed. Elsevier BV: Amsterdam, 2012; Vol. 2, pp 399–409.
21. Beaucage G, Ulibarri TA, Black EP, Schaefer DW, In *Hybrid Organic-Inorganic Composites*, American Chemical Society: 1995; Vol. 585, pp 97-111.
22. Lindner P, Zemb T, *Neutrons, X-ray and Light Scattering*. North Holland, Elsevier: Amsterdam, 2002.
23. Percus JK, Yevick GJ (1958) Physical Review 110:1-13
24. Ashcroft NW, Langreth DC (1967) Physical Review 156:685-692
25. Baeza GP, Genix AC, Degrandcourt C, Gummel J, Mujtaba A, Saalwächter K, Thurn-Albrecht T, Couty M, Oberdisse J (2014) ACS Macro Letters 3:448-452
26. Boonsomwong K, Genix A-C, Chauveau E, Fromental J-M, Dieudonné-George P, Sirisinha C, Oberdisse J (2020) Polymer 189:122168
27. Cattinari G, Steenkeste K, Le Bris C, Canette A, Gallopin M, Couty M, Fontaine-Aupart M-P (2021) J. Appl. Polym. Sci. 138:50221

28. McGreevy RL (2001) J. Phys. Condens. Matter 13:R877-R913
29. McGreevy RL, Pusztai L (1988) Molecular Simulation 1:359-367
30. Oberdisse J, Hine P, Pyckhout-Hintzen W (2007) Soft Matter 2:476-485
31. Musino D, Genix A-C, Chauveau E, Bizien T, Oberdisse J (2020) Nanoscale 12:3907-3915
32. Musino D, Oberdisse J, Farago B, Alegria A, Genix A-C (2020) ACS Macro Letters 9:910-916
33. Cerveny S, Bergman R, Schwartz GA, Jacobsson P (2002) Macromolecules 35:4337-4342
34. Kremer F, Schönhals A, *Broadband Dielectric Spectroscopy*. Springer-Verlag: Heidelberg, 2003.
35. Otegui J, Schwartz GA, Cerveny S, Colmenero J, Loichen J, Westermann S (2013) Macromolecules 46:2407-2416
36. Schwartz GA, Ortega L, Meyer M, Isitman NA, Sill C, Westermann S, Cerveny S (2018) Macromolecules 51:1741-1747
37. Souillard C, Chazeau L, Cavaillé J-Y, Brun S, Schach R (2019) Polymer 168:236-245
38. Zhuravlev LT (2000) Colloids Surf. A Physicochem. Eng. Asp. 173:1-38
39. Cerveny S, Schwartz GA, Otegui J, Colmenero J, Loichen J, Westermann S (2012) J. Phys. Chem. C 116:24340-24349
40. Meier JG, Fritzsche J, Guy L, Bomal Y, Kluppel M (2009) Macromolecules 42:2127-2134
41. Tsangaris GM, Psarras GC, Kouloumbi N (1998) Journal of Materials Science 33:2027-2037
42. Baeza GP, Oberdisse J, Alegria A, Couty M, Genix AC (2015) Phys. Chem. Chem. Phys. 17:1660-1666
43. Baeza GP, Oberdisse J, Alegria A, Saalwaechter K, Couty M, Genix A-C (2015) Polymer 73:131-138
44. Hernández M, Carretero-González J, Verdejo R, Ezquerra TA, López-Manchado MA (2010) Macromolecules 43:643-651
45. Steeman PAM, Maurer FHJ, Vanes MA (1991) Polymer 32:523-530
46. Steeman PAM, Baetsen JFH, Maurer FHJ (1992) Polymer Engineering & Science 32:351-356
47. Huang M, Tunnicliffe LB, Zhuang J, Ren W, Yan H, Busfield JJC (2016) Macromolecules 49:2339-2347
48. Roland CM (2016) Rubber Chemistry and Technology 89:32-53
49. Le HH, Qamer Z, Ilisch S, Radusch H-J (2006) Rubber Chemistry and Technology 79:621-630
50. Meier JG, Kluppel M (2008) Macromolecular Materials and Engineering 293:12-38
51. Böhning M, Goering H, Fritz A, Brzezinka KW, Turky G, Schönhals A, Schartel B (2005) Macromolecules 38:2764-2774
52. Ortega L, Cerveny S, Sill C, Isitman NA, Rodriguez-Garraza AL, Meyer M, Westermann S, Schwartz GA (2019) Polymer 172:205-212
53. Bocharov VN, Bureiko SF, Koll A, Rospenk M (1998) Journal of Structural Chemistry 39:502-507

54. Ortiz-Serna P, Díaz-Calleja R, Sanchis MJ, Floudas G, Nunes RC, Martins AF, Visconte LL (2010) Macromolecules 43:5094-5102
55. Hernández M, Ezquerra TA, Verdejo R, López-Manchado MA (2012) Macromolecules 45:1070-1075
56. Ikeda Y, Higashitani N, Hijikata K, Kokubo Y, Morita Y, Shibayama M, Osaka N, Suzuki T, Endo H, Kohjiya S (2009) Macromolecules 42:2741-2748
57. Lindemann N, Schawe JEK, Lacayo-Pineda J (2021) Journal of Applied Polymer Science 138:49769
58. Colmenero J, Arbe A (2007) Soft Matter 3:1474-1485
59. Genix AC, Arbe A, Alvarez F, Colmenero J, Willner L, Richter D (2005) Physical Review E 72:
60. Hoffmann S, Willner L, Richter D, Arbe A, Colmenero J, Farago B (2000) Physical Review Letters 85:772-775
61. Lodge TP, McLeish TCB (2000) Macromolecules 33:5278-5284
62. Adam G, Gibbs JH (1965) J. Chem. Phys. 43:139-146
63. Cangialosi D, Schwartz GA, Alegría A, Colmenero J (2005) J. Chem. Phys. 123:144908
64. Rathi A, Hernández M, Garcia SJ, Dierkes WK, Noordermeer JWM, Bergmann C, Trimbach J, Blume A (2018) Journal of Polymer Science Part B: Polymer Physics 56:842-854
65. Arrighi V, McEwen IJ, Qian H, Prieto MBS (2003) Polymer 44:6259-6266
66. Tsagaropoulos G, Eisenberg A (1995) Macromolecules 28:6067-6077
67. Mele P, Marceau S, Brown D, de Puydt Y, Alberola ND (2002) Polymer 43:5577-5586
68. Robertson CG, Lin CJ, Rackaitis M, Roland CM (2008) Macromolecules 41:2727-2731
69. Pissis P, Fragiadakis D, Kanapitsas A, Delides K (2008) Macromolecular Symposia 265:12-20
70. Fragiadakis D, Bokobza L, Pissis P (2011) Polymer 52:3175-3182
71. Robertson CG, Rackaitis M (2011) Macromolecules 44:1177-1181
72. Warasitthinon N, Robertson CG (2018) Rubber Chemistry and Technology 91:577-594
73. Kummali MM, Miccio LA, Schwartz GA, Alegría A, Colmenero J, Otegui J, Petzold A, Westermann S (2013) Polymer 54:4980-4986
74. Papon A, Montes H, Lequeux F, Oberdisse J, Saalwachter K, Guy L (2012) Soft Matter 8:4090-4096
75. Alvarez F, Alegra A, Colmenero J (1991) Physical Review B 44:7306-7312
76. Alvarez F, Alegría A, Colmenero J (1993) Physical Review B 47:125-130
77. Mujtaba A, Keller M, Ilisch S, Radusch HJ, Beiner M, Thurn-Albrecht T, Saalwächter K (2014) ACS Macro Letters 3:481-485
78. Papon A, Saalwächter K, Schäler K, Guy L, Lequeux F, Montes H (2011) Macromolecules 44:913-922
79. Richter D, Monkenbusch M, Arbe A, Colmenero J, *Neutron Spin Echo in Polymer Systems*. Springer Berlin Heidelberg, 2005; Vol. 174, p 1-221.

80. Musino D, Oberdisse J, Sztucki M, Alegria A, Genix A-C (2020) Macromolecules 53:8083-8094
81. Cheng S, Carroll B, Bocharova V, Carrillo J-M, Sumpter BG, Sokolov AP (2017) J. Chem. Phys. 146:203201
82. Genix A-C, Bocharova V, Kisliuk A, Carroll B, Zhao S, Oberdisse J, Sokolov AP (2018) ACS Applied Materials & Interfaces 10:33601-33610
83. Genix A-C, Bocharova V, Carroll B, Lehmann M, Saito T, Krueger S, He L, Dieudonné-George P, Sokolov AP, Oberdisse J (2019) ACS Applied Materials & Interfaces 11:17863-17872